ANL-77-35

HIGH-PERFORMANCE BATTERIES FOR STATIONARY ENERGY STORAGE AND ELECTRIC-VEHICLE PROPULSION

Progress Report for the Period January–March 1977

ARGONNE NATIONAL LABORATORY, ARGONNE, ILLINOIS

Prepared for the U. S. ENERGY RESEARCH AND DEVELOPMENT ADMINISTRATION under Contract W-31-109-Eng-38

Printed in the United States of America
Available from
National Technical Information Service
U. S. Department of Commerce
5285 Port Royal Road
Springfield, Virginia 22161
Price: Printed Copy $5.00; Microfiche $3.00

Distribution Category:
Energy Storage—Electrochemical
(UC-94c)

ANL-77-35

Argonne National Laboratory
9700 South Cass Avenue
Argonne, Illinois 60439

HIGH-PERFORMANCE BATTERIES FOR STATIONARY ENERGY STORAGE AND ELECTRIC-VEHICLE PROPULSION

Progress Report for the Period
January—March 1977

P. A. Nelson	Director, Energy Storage
N. P. Yao	Associate Director, Energy Storage
R. K. Steunenberg	Manager, Lithium/Metal Sulfide Battery Program
A. A. Chilenskas	Manager, Battery Commercialization
E. C. Gay	Section Manager, Battery Engineering
J. E. Battles	Group Leader, Materials Development
F. Hornstra	Group Leader, Battery Charging Systems
W. E. Miller	Group Leader, Industrial Cell and Battery Testing
M. F. Roche	Group Leader, Cell Chemistry
H. Shimotake	Group Leader, Cell Development and Engineering

June 1977

Previous Reports in this Series

ANL-76-35	January—March 1976
ANL-76-81	April—June 1976
ANL-76-98	July—September 1976
ANL-77-17	October—December 1976

PREFACE

The program on high-temperature secondary batteries at Argonne National Laboratory is carried out principally in the Chemical Engineering Division, with assistance on specific problems being given by the Materials Science Division and, from time to time, by other Argonne divisions. The individual efforts of many scientists, engineers, and technicians are essential to the success of the program, and recognition of these efforts is reflected by the individual contributions cited throughout the report.

TABLE OF CONTENTS

LIST OF FIGURES

LIST OF TABLES

HIGH-PERFORMANCE BATTERIES FOR STATIONARY ENERGY STORAGE AND ELECTRIC-VEHICLE PROPULSION

Progress Report for the Period
January—March 1977

ABSTRACT

This report describes the research, development, and management activities of the program at Argonne National Laboratory (ANL) on lithium-aluminum/metal sulfide batteries during January-March 1977. These batteries are being developed for electric vehicle propulsion and stationary energy storage. The present cells, which operate at 400-450°C, are of a vertically oriented, prismatic design with a central positive electrode of FeS or FeS_2, two facing negative electrodes of lithium-aluminum alloy, and an electrolyte of molten LiCl-KCl.

A major objective of this program is to transfer the technology to industry as it is developed, with the ultimate goal of a competitive, self-sustaining industry for the commercial production of lithium-aluminum/metal sulfide batteries. Technology transfer is being implemented by several means, including the assignment of industrial participants to ANL for various periods of time and the subcontracting of development and fabrication work on cells, cell components, and battery testing equipment to industrial firms.

Testing and evaluation of industrially fabricated cells is continuing. During this period, Li-Al/FeS and Li-Al/FeS_2 cells from Eagle-Picher Industries and Li-Al/FeS cells from Gould Inc. have been tested. The cells were tested individually and the Eagle-Picher cells were tested in parallel and series battery configurations. These tests provide information on the effects of design modification and alternative materials for cells. Improved electrode and cell designs are being developed and tested at ANL, and the promising designs are incorporated in the industrially fabricated cells. Among the concepts receiving major attention are carbon-bonded positive electrodes, scaled-up designs of stationary energy storage cells, additives to extend electrode lifetime, alternative electrode separators, and pellet-grid electrodes.

The materials development efforts include the development of a new, lightweight electrical feedthrough; studies of various current-collector designs; investigation of Y_2O_3 powder as separator material; wettability tests of materials for cell components; and postoperative examinations of cells. The cell chemistry studies were concerned with discharge mechanisms of FeS electrodes, with the mechanism of loss of sulfur and iron from FeS_2 electrodes, and with other transition-metal sulfides as positive electrode materials. The advanced battery effort investigated the use of calcium alloys for the negative electrode and the use of an iron current collector in the positive electrode.

SUMMARY

Commercial Development

A rough draft of a study to evaluate possible near-term markets for the lithium/iron sulfide battery is in progress. The size of the market (*i.e.*, total battery production capacity needed in a year) at a battery cost of $150/kW-hr is approximately 900 MW-hr/yr, and approaches that required for an automated battery plant.

The projected lifetime costs (initial and operating costs) for a lithium/iron sulfide battery-powered compact automobile are compared with those for a gasoline-powered compact automobile. The comparison shows that the cost of driving the electric car is about the same as, or slightly less than, driving the gasoline powered car with gasoline priced at today's rates.

An analysis comparing the cost of operating a diesel bus *vs.* a lithium/iron sulfide battery-powered bus has been completed. The comparison shows that, assuming an 80% federal subsidy to the bus operator for the diesel- and battery-powered buses, about $2000/yr can be saved by the use of the electric bus with power available at 1¢/kW-hr and about $500/yr with power at 2.5¢/kW-hr.

Systems design work was continued with the fabrication of the Mark 0 jacket for an electric-vehicle battery scheduled for completion about October 1977. This jacket is to be used for stationary testing in the laboratory.

A conceptual design/cost study for a 5.6 MW-hr truckable stationary energy storage module was nearly completed. This module consists of 168 cell stacks (8 cells per stack) that are vertically arrayed in a 6 x 28 grid. The cell to be used in this module contains 10 negative and 11 positive plates positioned horizontally, weighs about 55 kg, and delivers about 4.4 kW-hr at the 5-hr discharge rate.

The commercialization plan for lithium/metal sulfide batteries includes contractual arrangements with industrial firms to develop and fabricate cells, cell components, battery components, and battery testing equipment. Planning at Gould Inc. for 50 cells with hot-pressed FeS_2 positive electrodes having molybdenum current collectors was completed. At Eagle-Picher Industries, Inc., work is continuing on the production of 58 cells of both the FeS and FeS_2 type. Catalyst Research Corp. is continuing to develop simplified procedures for the fabrication of cells.

In contractual work directed toward separator development, the production and stockpiling of boron nitride roving is proceeding at about 15 kg/month at Carborundum Corporation. A paper-making trial run using BN fibers and asbestos fibers was successfully completed at the University of Florida. Samples of separators using BN fibers with organic binders were received for testing from Fiber Materials, Inc.

Industrial Cell and Battery Testing

A series of tests was completed in which Eagle-Picher FeS_2 cells of the Type 2B baseline design were cycled with various cutoff voltages. The conclusions drawn from these tests were: (1) operating with a charge cutoff voltage up to the maximum level allowable for FeS_2 cells did not shorten the cell lifetime but did increase the specific energy; (2) the series internal resistances of these cells were initially 8-10mΩ and they increased at the end of cell life; (3) shallow cycles interspersed with deep cycles (one deep cycle in every ten cycles) did not appreciably increase cell lifetime; (4) useful cell life was 85-125 days and 150-500 cycles, the latter including shallow cycles; and (5) cell and cycle life can be increased significantly by a very low charge rate (<4 A) and, therefore, possibly by constant voltage or tapering-charge modes.

Eagle-Picher cells that incorporate changes from the baseline design of the FeS cell are also undergoing testing. Cells in which yttria (Y_2O_3) felt was substituted for boron nitride (BN) cloth in the separator failed in less than 21 days. In addition, a second generation cell with a Y_2O_3-separator, which had a molded BN frame around the positive electrode to overlap the Y_2O_3 felt at the edge, was terminated after 65 days. These results indicate that Y_2O_3-felt separators cannot be used in cells of the present design. Other design changes involved reducing the thickness of the positive (from 0.63 to 0.56 cm) and the negative electrode (from 0.72 to 0.66 cm) as well as increasing the density of the negative electrode. This change increased the specific energy from 60 (baseline design) to 67 W-hr/kg (modified design) at a 10-hr rate for FeS cells.

Cell EP-2B8 was studied to determine the performance of a cell in an air atmosphere. This cell has now been operated in an air environment for more than 223 days, and is performing as well as identical cells operated in an inert atmosphere.

Thermal evaluation of an FeS_2 cell (EP-2B6) showed temperature changes of up to 15°C during cycling. A simple temperature control and cooling system will be sufficient to keep the battery within the desired temperature range.

Two Gould FeS cells (G-02-002 and G-03-002) have been qualification tested at ANL. These cells, one with $CaCl_2$ in the negative electrode and the other without $CaCl_2$, gave essentially the same performance. This design showed good potential and gave stable, reproducible cell performance for the period tested (67 days). Gould has operated two cells in their facilities with about the same results. This is now considered to be the baseline FeS cell design for 12.7 x 17.8 cm cells.

Testing of cells in a series arrangement was conducted to study the interactions of the cells and to establish data for the scale-up of battery designs. Tests were performed on Battery B7-S (two type B FeS cells in series) to determine the effect of intermediate shallow cycling on subsequent deep cycling. After more than 115 cycles at a 5-hr discharge rate followed by a 6-hr bulk charge and 4-hr equalization charge, a decrease in performance resulted owing to insufficient equalization charge time. After several cycles using 10-hr equalization times, the performance returned to its previous value.

Battery B7-S has now operated for more than 295 days and 472 cycles. Start-up and conditioning of the first six-cell Li-Al/FeS_2 battery (B10-S) was completed in a test chamber. For the first four cycles at low currents the peak specific energy (based on cell weight) was ∿87 W-hr/kg at about a 16-hr rate. After cycling in the test chamber, these six cells were placed in a vacuum insulated housing; performance and temperature measurements were then made. The case provided good insulation: with a battery temperature of 435°C, the external temperature of the case was <25°C. The power necessary to maintain the battery at ∿435°C was 57-60 W.

Battery Charging Systems

Proposals were received to complete a cost and design study of a full-scale battery system for the Li-Al/FeS_2 battery, and a procurement package is being prepared. A monitor and equalizer control system has been placed in operation on a six cell Li-Al/FeS_2 battery, and is performing well. Construction of a 100-A cell and battery cycler, that will handle four Li-Al/FeS_2 cells in series, was started. One of the 25-A "mini-cyclers" has been modified to allow cell charging in either a constant current or constant voltage mode.

Cell Development and Engineering

This part of the program is directed toward the development and testing of Li-Al/FeS_x cells having improved performance and lower cost. The work is concentrated on cells that are adaptable to the electric vehicle.

Two upper-plateau FeS_2 cells were built with Li_2FeS_2 ("X-phase") as the starting material in the positive electrode. Because Li_2FeS_2 is relatively unaffected by air or moisture, one of the cells was fabricated in air and helium atmosphere and the other cell just in air. The results were promising, and scale-up is under way.

Four uncharged, Upper plateau FeS_2 cells were tested. The amounts of lithium and aluminum in the negative electrodes varied from 0 to +50%. The higher lithium and aluminum concentrations yielded better FeS_2 utilization.

Carbon-bonded positive electrodes using FeS or FeS_2 as the active material continue to show promise. Cell CB-1, a charged cell with a carbon-bonded $CuFeS_2$ electrode, has accumulated 427 days and 736 cycles with only 15% decline from its typically high value of 67 A-hr at the 5-hr discharge rate. Cell KK-5, an uncharged FeS cell with a Cu_2S additive, has completed 460 cycles in 333 days; its 90 A-hr capacity had diminished by less than 10% when it attained a lifetime goal of 400 cycles. A new design of a molybdenum current collector with a welded connection has reduced the resistance of the KK-series cells (carbon-bonded electrodes) from 6-8 to 4.5mΩ.

Tests were performed on two cells, M-1 and M-2, with charged FeS_2 electrodes and Y_2O_3-felt separators. The major difference between the two cells was in the housing. In Cell M-2 the current collector trays in the negative electrode were part of the housing, and this made the cell lighter. Although Cell M-1 developed a short circuit after 17 days, it showed good upper-plateau performance, with a specific energy of 98 W-hr/kg at a 25-A discharge rate (∿90 mA/cm^2). Cell M-2 has been in operation more than 14 days, and has shown slightly improved performance over Cell M-1.

Investigation is continuing on the addition of a third metal to the Li-Al alloy negative electrode in engineering-size (13 x 13 cm) cells, designated the FM series. Cell FM-3, which has negative electrodes of Li-Al-8 wt % Sn, was still in operation after 186 cycles and 109 days; its capacity has declined from 57 to 50 A-hr. The capacity of Cell FM-3 is significantly greater than the capacity of either Cell FM-1 (In additive in the negative electrode) or Cell FM-2 (Ca additive in the negative electrode).

Five engineering-size cells (TO-series) with nonwoven cloth separators have been built and tested. The tests showed that Y_2O_3- and BN-felt separator/retainers have many advantages over BN and ZrO_2 cloth separator/retainers. A compact, engineering-scale cell with a Y_2O_3 powder separator is presently in operation; the early cell performance looks very promising.

Materials Development

The development of a lightweight, low-cost, and leak-tight electrical feedthrough is continuing. The most outstanding success has been with the crimp-type mechanical feedthough developed at ANL. The crimp-type feedthrough for a 1/4 in. (6.35 mm) dia. conductor has a weight of 46 g and a projected cost of only $1.14. Leak rates are about 10^{-6} Pa m^3/sec without, and about 10^{-10} Pa m^3/sec with, a secondary seal of solder glass. It is anticipated that this type of feedthrough will be installed in the Mark I electric-vehicle cells.

One of the higher cost materials of the LiAl/LiCl-KCl/FeS_2 cells is the current collector for the FeS_2 electrode. The following current-collector designs were studied to determine their costs: flat-sheet molybdenum, honeycomb molybdenum, and molybdenum porous metal. This study showed that the honeycomb design meets our earliest (1981) cost goals, whereas the porous metal and flat-sheet designs meet our intermediate (1985) cost goals. None of these designs meet our long range (1990) goals. A few industrial contractors have submitted proposals for development of lower cost current collectors for the FeS_2 electrode. These proposals, most of which involve molybdenum bonding, are in various stages of evaluation.

A powder separator is being developed as an alternative to the BN fabric currently used in Li-Al/FeS_x cells. A horizontal cell, with an all-powder separator and no frame and screen assembly around the positive electrode, operated successfully for 41 days before the test was voluntarily terminated. Cell performance was excellent. Postoperative examination showed that the separator had maintained its integrity and had been effective in retaining the active materials within the electrode. These data indicate that it may be possible to eliminate the frame and screen assembly in the positive electrode with the use of all-powder separators.

An experimental apparatus was constructed to measure permeability to gas flow of rigid separator candidates; preliminary measurements were made on specimens prepared by incorporating volatile organic materials with Y_2O_3 powder prior to pressing. Additional flowmeters are being added to the permeability apparatus to improve the accuracy of measurements over a broader range of flow conditions.

A commercial device is being used to produce preformed foam by mixing ceramic suspensions with preformed foam; the foam structure is solidified by reaction of the powder particles in dilute nitric acid.

An experimental alloy with a composition of Fe-30 wt % Ni-15 wt % Mo was received for evaluation as a possible current-collector material. The fabrication difficulties encountered by the vendor in rolling this material into a 0.25 mm sheet were a result of the presence of a second phase, which was apparently caused by insufficient homogenization of the starting ingot. This phase was eliminated by solution annealing at 1225°C. Corrosion tests on annealed samples indicated that the alloy should be suitable for application in FeS cells.

Further studies have been conducted on the wettability of porous separator materials by molten-salt electrolyte. Lithcoa LiCl-KCl was more effective in wetting hot-pressed boron nitride surfaces than the Anderson Physics Laboratories' LiCl-KCl. Aluminum nitride appears to be more difficult to wet than boron nitride, but it is less susceptible to subsequent dewetting. Other surface studies showed that the tendency of the LiCl-KCl electrolyte to creep on metal surfaces is increased markedly by the addition of LiAl alloy to the salt.

Owing to the degassing and attendant pressure buildup that can occur during the operation of a cell, a study was begun to characterize (by mass spectrometry) the gaseous species produced while cells are in a charge, discharge, or open-circuit mode. In addition, because the electrical resistances of the various components of a cell affect efficiency, a study was initiated on the electrical conductivity of dispersions of nonconducting solids in molten LiCl-KCl.

Major changes in handling procedures for metallographic samples have made possible the preparation of cell samples suitable for analyses by the Ion Microprobe Mass Analyzer. This technique will permit analyses such as the Li:Al ratios of the metallic particles in the negative electrodes of Li-Al/FeS_x cells.

Postoperative examinations were completed on eleven engineering-scale cells during this period. Tests of these cells were terminated because of short circuits or declining performance. The major causes of the short circuits were: (1) extrusion of active materials of one electrode into the opposite electrode because of inadequate mechanical restraint and (2) build up of metallic particles within the separator. Metallographic examinations of FeS_2 cells have shown the presence of Li_2S-iron precipitates in the separator. The formation of the Li_2S appears to be related to the high sulfur activity in the FeS_2 cells.

Cell Chemistry

Studies of sulfur and iron losses from FeS_2 electrodes were conducted. A rapid decrease in the sulfur-iron ratio of FeS_2 was found when an open crucible containing a mixture of Li_2S and FeS_2 was heated in LiCl-KCl electrolyte at 700 K. Thermodynamic calculations indicate that the vapor pressure of sulfur over Li_2S and FeS_2 mixtures is high enough to account for the observations. Measurements of the sulfur and iron concentrations of

LiCl-KCl electrolyte in contact with Li_2S-FeS_2 mixtures did not reveal an unusually high solubility; however, the solutions became intensely colored (yellow-orange). These results suggest that Li_2S in a BN separator will not be readily absorbed by a positive electrode that is rich in FeS_2.

A study was conducted on TiS_2 as an alternative to FeS or FeS_2 in positive electrodes. Tests of a 1 A-hr TiS_2 cell indicated that this electrode operates well. Large scale tests were then undertaken, and a 142 A-hr LiAl/TiS_2 cell was constructed. Its capacity at the 10-A rate was 90 A-hr (54 W-hr/kg). This system appears to be promising.

It is suspected that the decreasing capacity of the Li-Al electrodes results from morphological changes of the active material over a period of time. Thus studies were conducted on the use of various metallic additives to the Li-Al alloy as a means of controlling these morphological changes. Additions of lead (10 wt %), tin (5 wt %), or copper (5 wt %) did not improve the capacity retention of the electrode. However, the addition of indium (1 wt %) greatly improved capacity retention.

Advanced Battery Research

Cyclic voltammetry is being used to study the electrochemical behavior of candidates for electrode materials. Results for Ca-Al, Ca-Mg, Ca-Mg-Si, and FeS electrodes in LiCl-KCl-$CaCl_2$ electrolyte are reported. The calcium negative electrodes gave somewhat lower utilizations than those obtained with LiAl negative electrodes in LiCl-KCl electrolyte. In-cell tests demonstrated that the Ca-Mg-Si negative electrode performs better than the Ca-Al or the Ca-Mg. The cyclic voltammogram of the FeS electrode helped to identify a significant side reaction in the calcium cells--the formation of $FeCl_2$ by oxidation while FeS is being generated from iron and CaS. This side reaction was suppressed by use of a carbon instead of an iron current collector for the FeS electrode in the calcium system.

Positive electrodes of FeS or FeS_2 having capacities of 1 to 2 A-hr were prepared in small, graphite housings. The negative electrodes consisted of Li (LiCl-KCl electrolyte), $CaAl_2$ (LiCl-KCl-$CaCl_2$), or Mg (NaCl-KCl-$MgCl_2$). Studies of these cells indicated that the calcium and magnesium electrodes require added current collector, such as distributed carbon powder throughout the active material, to obtain adequate utilization. The utilization for the lithium electrode was adequate.

Two uncharged, prismatic Mg_2Si/Fe(CaS) cells of 134 A-hr theoretical capacity were fabricated and tested. Their achieved capacities were about 50 A-hr. These cells employed mainly iron current collectors in their positive electrodes. Cells employing carbon current collectors are being designed.

Cell and Battery Development at Atomics International

Work is in progress on the construction of compact, uncharged bicells with AlN powder separators; one cell of this type has completed 113 cycles and 100 days of operation with 99% coulombic efficiency.

Operation of a 1.0 kW-hr Li_4Si/FeS-20 mol % Cu_2S cell was terminated after 330 cycles and 142 days. Postoperative examination disclosed that the probable causes of cell failure were (1) migration of copper from the positive electrode and (2) corrosion of the BN-cloth separator which had been plasma sprayed with $MgO \cdot Al_2O_3$ spinel.

An instrumented 1.0 kW-hr cell with a large number of thermocouples within the cell is being placed in operation. Data will be collected for determining thermal gradients in large load-leveling cells. Design of a 2.5 kW-hr pre-prototype cell for load-leveling is under way.

I. INTRODUCTION

Lithium-aluminum/metal sulfide batteries are being developed at Argonne National Laboratory (ANL) for use as (1) power sources for electric vehicles, and (2) stationary energy storage devices for load-leveling on electric utility systems and storage of electrical energy produced by solar, wind, or other sources. Performance and lifetime goals for the electric vehicle batteries and stationary energy storage batteries are listed in Table I-1. These goals are the same as those presented in the preceding report of this series (ANL-77-17, p. 8). However, future revision of the goals may be appropriate as the requirements of these two applications are investigated in greater detail through systems design studies.

Table I-1. Performance Goals for Lithium-Aluminum/Metal Sulfide Batteries

	Electric Vehicle Propulsion		Stationary Energy Storage	
Battery Goals	Mark I 1978	Prototype 1985	BEST 1982	Prototype 1985
Power				
Peak	30 kW	60 kW	1.5 MW	25 MW
Sustained Discharge	12 kW	25 kW	1 MW	10 MW
Energy Output	30 kW-hr	45 kW-hr	5 MW-hr	100 MW-hr
Specific Energy,[a] W-hr/kg	110	180	60-80	60-150
Discharge Time, hr	4	4	5	5-10
Charge Time, hr	8	5-8	8	10
Cycle Life	300	1000	1000	3000
Cost of Cells, $/kW-hr	-	35	25-30[b]	20

[a] Includes cell weight only; insulation and supporting structure is approximately 25% of total weight for the Mark I electric vehicle battery and 15 to 20% for the 1985 prototype vehicle battery.

[b] Projected cost at a production rate of 2000 MW-hr/yr.

Because of the markedly different performance, lifetime, and cost requirements for the electric vehicle and stationary energy storage applications, a clear-cut distinction is being made in the design characteristics of the cells and batteries that are being developed for these two purposes. The FeS_2 positive electrode is currently favored for the electric vehicle battery in view of its high specific energy and specific power. The FeS positive electrode appears to be better suited to the stationary energy storage application because of its longer lifetime and potential for low cost.

The Mark I electric vehicle battery, which will be the first full-scale (30-50 kW-hr) lithium-aluminum/metal sulfide battery of this type, is scheduled for testing in 1978, first in the laboratory and later in a van.

A conceptual design of this battery has been completed, and detailed design studies have been initiated. A plan is also under way for development and fabrication of cells, an insulated battery housing, and auxiliary equipment. This plan will also provide for the test equipment and procedures to be used with the Mark I battery. Before the Mark I battery is assembled, present plans call for a preliminary test (Mark 0) in which a partial loading of cells will be operated in the full-scale insulated housing for the Mark I battery.

Design considerations indicate that relatively small (*e.g.*, 13 x 18 x 2 cm, ∿150 A-hr) cells with one central positive electrode and two facing negative electrodes would be desirable for the electric vehicle battery. Modules of three parallel-connected cells would be connected in series to form the battery.

Conceptual design studies of a 5.6-MW battery module for stationary energy storage applications have also been completed. The module consists of a weatherproof insulated housing that can be transported to the point of use by truck, where the cells are inserted to form the battery. The present design concept for this unit involves multielectrode Li-Al/FeS cells having the configuration of a 25-cm cube.

The battery development program includes both an in-house research and development effort at ANL and subcontracts with several industrial laboratories. The ANL effort involves cell chemistry studies, materials development and evaluation, cell and battery development, industrial cell and battery testing, and commercialization studies. A small effort is also in progress at ANL on advanced battery systems that utilize low-cost, abundant materials. The major industrial subcontractors are the Atomics International Division of Rockwell International, Carborundum Co., Catalyst Research Corp., Eagle-Picher Industries, Inc., and Gould Inc. Atomics International is conducting a general research and development program with current emphasis on Li-Si/FeS cells for stationary energy storage applications. The Carborundum Co. is producing boron nitride fibers for electrode separators. Catalyst Research, Eagle-Picher, and Gould are involved primarily with the development and fabrication of cells that are tested either at ANL or in their own laboratories.

II. COMMERCIAL DEVELOPMENT
(A. A. Chilenskas)

The objective of the commercialization effort is the establishment of a competitive, self-sustaining industry capable of producing a supply of lithium/metal sulfide batteries that meets national needs. This objective is to be accomplished through normal market forces, with a minimum of governmental support. A commercialization plan is under development that will define the essential elements, *i.e.*, the market, product, and need (driving force for change). An essential part of this plan, the market study, is in a rough draft form; ANL is leading the study and assistance is being given by several industrial participants. The study will be a combination of a market survey and an economic analysis. The market survey will identify high-performance battery needs in military, aerospace, and industrial applications for the near term (1978-1985). The economic analysis will permit a projection of (1) the required production rates of lithium/iron sulfide batteries to satisfy the market for each year and (2) the capital expenditure requirements to support these production rates. In this way, the near-term markets will be used to build an industrial manufacturing base with a minimum of federal support.

A. Commercialization Studies
(A. A. Chilenskas, S. H. Nelson*)

1. Market Studies

A rough draft of a study to evaluate possible near-term markets for the lithium/iron sulfide battery is in progress. Preliminary estimates of the annual market for various market sectors are shown in Table II-1.

Table II-1. Possible Near-Term Markets for the Lithium/Iron Sulfide Battery

Market Sector	Price $/kW-hr	Size of Market,[a] MW-hr/yr
Submarines	250	107
Mobile Missile Launchers	180	60-160
Postal Vans and Trucks	170	98-198
Postal Vehicles and Buses	160	345-445
Postal Vehicles, Buses, Mining	150	795-895

[a]Preliminary estimates, January 1977.

As can be seen from this table, the size of the market is substantial at a battery cost of $150/kW-hr, *i.e.*, ∿900 MW-hr/yr, and approaches that required for an automated battery plant (1100 MW-hr/yr[1]).

*A member of the ANL Energy and Environmental Systems Division.

2. Cost of Driving Electric Automobiles

The projected lifetime (initial & operating) costs for a lithium/iron sulfide battery-powered compact automobile are compared with those for a gasoline-powered compact automobile in Table II-2. It was assumed that the

Table II-2. Projected Lifetime Costs for Compact Automobiles (1977 Dollars)

Cost Item	Gasoline-Powered Auto	Lithium/Metal Sulfide Battery Electric Auto
Depreciation Period, yr	10	12
Initial Vehicle Cost	$ 3,500	$4,375
Initial Battery Cost[a]	---	1,500
Repairs/Maintenance/Tires[b]	2,885	1,596
Pollution Control[b]	1,023	---
Insurance/Garaging/Taxes/Fees[b]	5,163	6,318
Gasoline[c]	1,666	---
Electric Power[d]	---	400-1,109
Financing Charge[e]	1,120	1,400
Investment Opportunity Loss[f]	1,168	3,609
Total Lifetime Cost	17,037	$19,198-19,907
Average Lifetime Cost, ¢/mile	17	16.0-16.6

[a] 30 kW-hr at $50/kW-hr ($35/kW-hr, factory price).

[b] Based on information in Ref. 2.

[c] $0.50/gallon at 30 mpg.

[d] Off peak $0.01-0.028/kW-hr at 0.33 kW-hr/mile.

[e] 15% at 2 yr.

[f] 7%.

first cost of the electric automobile is 25% higher than that of the gasoline automobile. This cost differential is somewhat offset by a 12-yr lifetime for the electric auto as compared with a 10-yr lifetime for the gasoline-powered auto. The battery lifetime is assumed to be 10 yr (~1000 deep discharge cycles) and the salvage value is equated to 2 years of depreciation cost. Other important assumptions are given in Table II-2. The justification for the use of $0.01-0.028/kW-hr for the electric-energy cost is based upon the assumptions that night-time charging is employed and that the off-peak electrical rates are those found in a recent unpublished survey of off-peak pricing by S. H. Nelson. A summary of results from this survey is given in Table II-3.

The results of the cost analysis in Table II-2 indicate that the cost of driving a compact electric car is about the same as that for a compact,

Table II-3. Rates For Off-Peak Electricity

Utility	Source	Rate, ¢/kW-hr
Wisconsin Electric Power	PSCW Docket 6630-ER-2	0.94
Northern States Power Co. (Minnesota)	Electric Rate Book	1.00
Virginia Electric Power	Letter To State Corporation Council	1.00
Consolidated Edison	PSCNY Case 26806	2.56
Madisons Gas and Electric Co.	PSCW Docket 3270-UR-1	0.90
Wisconsin Power And Light	PSCW Docket 3-U-8505	0.85
San Diego Gas And Electric Co.	Publication-State Energy Commission	2.70

efficient (30 mpg) gasoline-powered car with gasoline prices at about today's rates ($0.50/gallon, tax-free basis). If gasoline prices increase more rapidly than the price of electricity, as is likely, then the electric automobile will be increasingly favored in terms of driving cost per mile.

3. Operating Cost of a Diesel Bus *vs.* an Electric Bus

An analysis comparing the cost of operating a diesel bus *vs.* a lithium/iron sulfide battery-powered bus has been completed. The analysis assumes that a first-generation battery costs $150/kW-hr, that it has a 7-yr life, and that it is replaced with a second-generation battery with a 10-yr life that costs $50/kW-hr. A federal subsidy of 80% is used for both the diesel and electric buses. Other important cost assumptions are given in Table II-4. The costs for the two types of vehicles, based upon a

Table II-4. Cost Comparison of Diesel *vs.* Electric Bus[a] (1976 Dollars)

Cost Element	Diesel	Electric
Bus	$75,000	$90,000
Battery		
1st Generation ($150/kW-hr, year 1-7)	---	60,000
2nd Generation ($50/kW-hr, year 8-15)	---	20,000
Fuel Costs, per mile	10¢	4-10¢
Operating & Maintenence, per mile	17¢	10¢
Lifetime, years	10	15

[a]Forty-five passenger

present-value analysis with the discount rate at 10%, are given in Table II-5. With electricity prices at 1¢/kW-hr important substantial savings are projected for the battery-powered bus; there would be lesser savings with electricity priced at 2.5¢/kW-hr. This analysis suggests that the electric-bus market should be considered as a near-term market for a battery developer because of the potential savings possible for the bus operator.

Table II-5. Annual Costs for Bus Operation (1976 Dollars)

	Diesel	Electric	
Bus Depreciation[a],	1500	1200	
Battery Depreciation[b]			
1st Generation (year 1-7, $150/kW-hr)	--	1715	
2nd Generation (year 8-15, $50/kW-hr)	--	2000	
Fuel Cost			
Diesel at 40¢/gal	3000	--	
Electric at 1¢/kW-hr	--	1200	
Electric at 2.5¢/kW-hr	--	3000	
Operating and Maintenance	5100	3000	
Total Annual Costs		1¢/kW-hr	2.5¢/kW-hr
Diesel	9600	--	--
Electric			
with 1st Generation Battery	--	7115	8915
with 2nd Generation Battery	--	7400	9200

[a]An 80% Federal Subsidy is assumed.

[b]An 80% Federal Subsidy is assumed for the 1st generation battery, with no subsidy for battery replacement.

B. Systems Design

(A. A. Chilenskas, T. E. Fornek*, K. Gentry†
M. A. Slawecki, F. Hornstra, R. F. Malecha)

1. Electric Vehicle Batteries

A joint effort between ANL and Eagle-Picher is being directed towards the design of a battery jacket for a 30 kW-hr electric-vehicle battery. An insulating jacket, designated Mark 0, is to be used in stationary testing in the laboratory. This testing is directed mainly towards the thermal evaluation of the vacuum-foil insulation and the use of once-through ambient air cooling for battery temperature control. Fabrication of this jacket is scheduled for completion about Jan. 1978.

*ANL Engineering Division

†Eagle-Picher Industries, Inc.

2. Truckable Utility Module

A conceptual design/cost study of a 5.6 MW-hr truckable battery module to be used for stationary energy storage is nearing completion. The conceptual design has been completed and a cost analysis is under way.

The conceptual design of a cell to be used in the truckable battery module is shown in Fig. II-1. The cell configuration is cubic with an

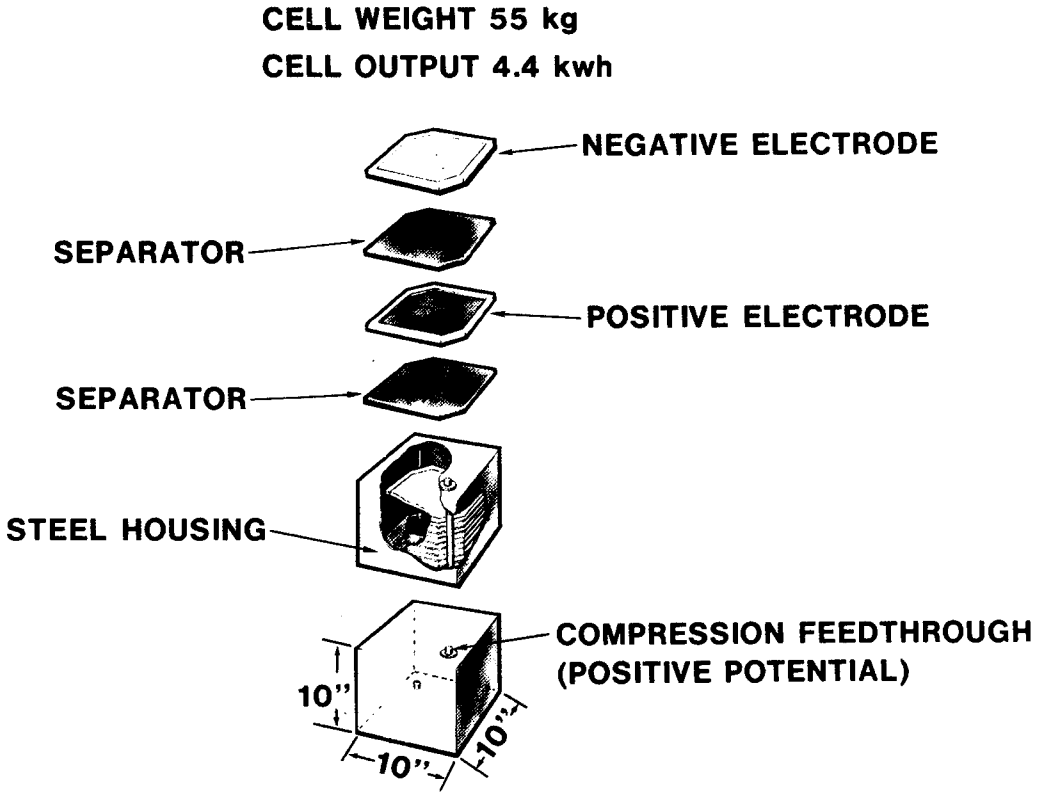

Fig. II-1. Design of Cell for Stationary Energy-Storage Battery

approximate dimension of 25 cm on a side. The cell contains about 10 negative and 11 positive plates positioned horizontally. The cell weight is about 55 kg including the mild-steel housing and the compression feedthrough. The cell is designed to deliver about 4.4 kW-hr at the 5-hr discharge rate. The basic replaceable battery element is designated the cell stack, and is shown in Fig. II-2. It is designed to be removed and replaced with a similar element, if required, while the battery is at operating temperatures by the use of an insulated cask. The stack contains 8 cells weighing 440 kg, and delivers 35 kW-hr at the 5-hr rate. The conceptual design of the truckable module for a stationary energy storage battery is shown in Fig. II-3. The module consists of a weatherproof housing that is small enough to be trucked to the point of use. It consists of 168 cell stacks that are

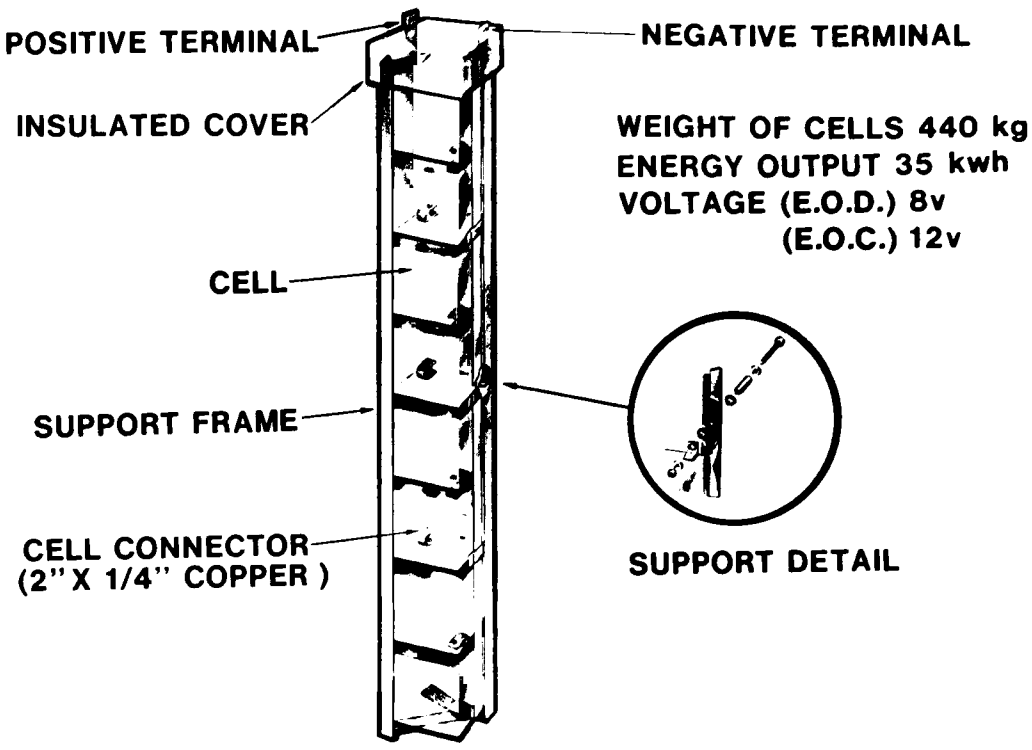

Fig. II-2. Cell Stack for Stationary Energy-Storage Battery

vertically arrayed in a 6 x 28 grid arrangement and delivers about 5.6 MW-hr at the 5-hr rate. Provisions for central instrumentation, heating and cooling equipment, and charging equipment are included within the housing.

C. Industrial Contracts

1. Cell and Battery Development Contracts
(R. F. Malecha, R. E. Elliott)

The industrial effort to develop manufacturing techniques and procedures for the design, fabrication and testing of cells is continuing under contracts with Gould Inc., Eagle-Picher Industries, Inc., and Catalyst Research Corporation.

Gould has completed the planning necessary to fabricate 50 upper plateau, uncharged cells with 13 x 18 cm hot-pressed FeS_2 positive electrodes having molybdenum current collectors. The cells are to be fabricated in accordance with a requirements matrix that provides for varied compositions and thicknesses of electrodes. Materials have been ordered with the longest lead-time item, molybdenum honeycomb, expected in late April. A facility is being installed for the simultaneous testing of 10 cells. The test equipment components are being ordered on a cost-sharing basis between Gould and ANL.

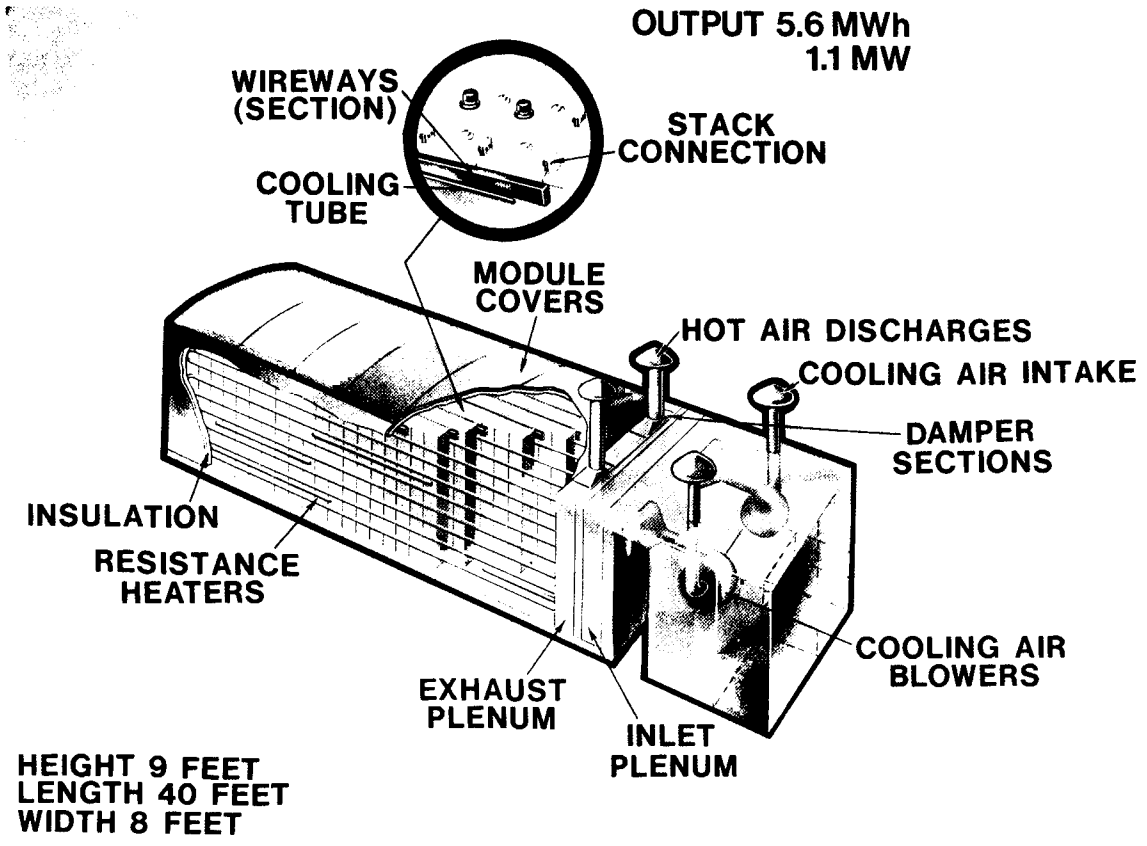

Fig. II-3. Truckable Module for Stationary Energy-Storage Battery

At Eagle-Picher, work is continuing on the production of 58 cells; these cells are of a mixed variety, *i.e.*, FeS and FeS_2 types that are either charged or uncharged. The requirements for the last 24 cells in the group have been defined, and include an improved design for attaching a honeycomb to the positive current lead. The glove-box facility used for the ANL work has been moved to a larger work area in a dry room. The move was necessitated by the additional glove boxes recently purchased for installation in the facility. A 500-ton (4.5×10^5 kg) press needed to produce 13 x 18 cm cold-pressed electrodes is being fabricated for delivery to Eagle-Picher in June.

Work on the development of techniques for casting Li-Al electrodes in metal substrates has continued at Catalyst Research. Both nickel Retimet* and stainless steel expanded metal are being considered for the substrate. The new glove-box facility has recently been installed to handle phases of the work not suited to the dry-room atmosphere. Laser welding of molybdenum current collector parts is under investigation.

*A product of Dunlop, Ltd., Coventry, England

The first phase of a design study of hardware for a 30 kW-hr battery has been completed by Eagle-Picher. As a result of the preliminary design review, it was decided to pursue additional design and development ideas, including methods of connecting cell leads to a bus bar. This phase of the work is expected to begin in April. Final design work and planning for fabrication is scheduled for October. The design of the insulated battery container vessel is being investigated by other contractors, with Eagle-Picher responsible for the interface with the battery design.

2. Electrode Separators
(J. E. Battles)

The Carborundum Co. The production and stockpiling of boron nitride roving is proceeding at the rate of about 15 kg/month. The material is being stockpiled as roving in order that it may be converted to either fabric or felt separators as the particular application requires. The R&D contract for the development of BN-bonded felts was terminated in Nov. 1976. However, Carborundum has done additional work in this area. A large number of samples with different thicknesses and densities were supplied for ANL evaluation. Based on our evaluation of these samples, a purchase order was placed for about 4.65 m^2 of BN felt separator materials having a bulk density of about 8% and thicknesses of 0.7, 1.4, and 3.0 mm.

University of Florida.* Relocation and set-up of the continuous paper-making machine was completed. The initial trial run using unfired BN fibers and 15 wt % asbestos fibers was successfully completed. Additional runs using Y_2O_3 fibers and 15 wt % asbestos fibers were less successful because of the fragile nature of the Y_2O_3 fibers. Efforts are now under way to make a quantity of separator material for in-cell testing using fired BN fibers with 15 wt % asbestos fibers as the binder.

Fiber Materials, Inc. Fiber Materials, Inc. has provided separator samples that were prepared using varying lengths of BN fibers with organic binders. Thermal treatment of these samples for binder removal resulted in an extremely weak structure. The preliminary evaluations of these samples indicate that this approach for fabricating separators is unlikely to be successful.

*Contract funded directly by ERDA.

III. BATTERY ENGINEERING
(E. C. Gay)

Battery engineering includes (1) testing of industrially fabricated Li-Al/FeS_x cells and batteries assembled from these cells, (2) development of electrode and cell designs to meet the electric vehicle and stationary energy storage goals for cell performance, (3) improvement of cell-fabrication techniques, and (4) development of cell designs that use lower cost cell components. A summary of large scale cell tests is presented in Appendix A. Statistical data for the cell tests are given in Appendix B.

A. Industrial Cell and Battery Testing
(W. E. Miller)

1. Testing of Contractor-Produced Cells
(R. C. Elliott, W. E. Miller, R. Thompson,* P. F. Eshman, V. M. Kolba, G. W. Redding, J. L. Hamilton)

A performance summary of contractor-produced cells is presented in Appendix A. Some of these are "baseline cells," *i.e.*, they have been qualified by testing a series of cells of the same design to obtain baseline performance data. In later cells, design modifications were made, and the effects of these design modifications were determined by comparing cell performance to that of the baseline cells. The design features of the baseline Eagle-Picher cells were discussed previously (ANL-76-98, p. 15-17).

a. Eagle-Picher Cells

Testing of Eagle-Picher Cell 2B7 (a baseline FeS_2 cell with thick electrodes) was terminated after 525 cycles and 106 days. After the 30th cycle the cell was operated under a recently established seven-day cycling schedule (see Table III-1, ANL-77-17, p. 20). This was the last of a series of tests of Eagle-Picher type B baseline FeS_2 cells. The conclusions drawn from these tests were as follows: (1) operating with a charge cutoff voltage up to the maximum level allowable for FeS_2 cells did not shorten the cell life, but did increase the specific energy; (2) the series internal cell resistances were initially 8-10 mΩ, and then increased significantly at the end of the cell life; (3) shallow cycles interspersed with deep cycles (one deep cycle of greater than 50% utilization every ten cycles) did not appreciably increase cell lifetime; (4) useful cell life (*i.e.*, that part of the cycle life during which the cell retains 80% of its initial stable, but not peak, capacity) was 85-125 days and 150-500 cycles (the latter including shallow cycles); and (5) cell and cycle life can be prolonged significantly by a very low charge rate (<4 A) and, therefore, possibly by constant-voltage or tapering-charge modes.

At present, Eagle-Picher cells that incorporate changes from the baseline design are undergoing testing. The first cells from the contractor in which Y_2O_3 felt was substituted for the BN cloth of the separator failed in less than 21 days (Eagle-Picher Cells I-1-A-1, I-1-A-2, I-2-1 and I-2-2). Tests on these FeS cells which were carried out prior

*Industrial Participant from Gould Inc.

to their failure showed that the performance was essentially the same as that of the baseline FeS cells, namely, 60-65 W-hr/kg at the 10-hr rate. Cell EP-I-1-B-1 was a second-generation, Y_2O_3-separator cell with a molded BN frame around the positive electrode to overlap the Y_2O_3 felt at the edge; operation of this cell was terminated after 66 cycles and 65 days when coulombic effiency dropped sharply. Although the postoperative analyses of these cells by the Materials Group are not yet complete, the indications are that Y_2O_3 felt separators cannot be used in cells of the present design. Modifications in cell design appear to be needed to accommodate Y_2O_3-felt separators.

A second design change from the Type B baseline FeS_2 cells was an increase in the size of the positive terminal rod from 0.48 cm (3/16 in.) to 0.64 cm (1/4 in.) dia. This modification had no significant effect on the performance of these cells (EP-I-3-A-1, EP-I-3-A-2). The resistances of these cells were essentially the same as those of the baseline cells; this indicates that the controlling resistance was not in the terminal rod.

Other design changes from baseline cells involved decreases in the thicknesses and porosities of the electrodes. Cells EP-I-3-B-1 and EP-I-3-B-2 have a slightly thinner positive electrode and slightly denser and thinner negative electrodes than those used in the baseline cells. In the baseline cells, the positive electrode was 0.63 cm thick with a capacity of 78.0 A-hr; and the negative electrodes were 0.72 cm thick with a total capacity of 78.0 A-hr. In the I-3-B cells, the positive electrode was 0.56 cm thick with a capacity of 63.5 A-hr; and the negative electrodes were 0.66 cm thick with a total capacity of 85 A-hr. Preliminary tests of these cells show an increased specific energy (67 *vs.* 60 W-hr/kg at the 10-hr rate) and improved utilization of the positive electrode (84 *vs.* 70% at the 10-hr rate).

b. Gould Cells 02-002 and 03-002

Gould Inc. delivered two baseline-design cells (G-02-002 and G-03-002). These cells had 13 x 18 cm hot-pressed, uncharged electrodes. The active materials present initially in the positive electrode were a mixture of Li_2S, Fe, and Cu. The negative electrodes contained Li-Al with a lithium content of 8 at. %. This electrode composition approximates the lithium content of a fully discharged negative electrode. Cell G-02-002 contained $CaCl_2$ in the negative electrode. This addition was made to test a postulate that $CaCl_2$ would affect the morphology of the negative electrode in such a way as to increase cell lifetime. This cell also incorporated a new hermetic positive feedthrough (a joint development of Gould and ANL). Cell G-02-002 weighed 2.75 kg and Cell 03-002 weighed 2.73 kg.

Qualification tests of Cells G-02-002 and G-03-002 showed nearly identical performance. A specific energy of 58 W-hr/kg was measured at a 10-hr discharge and 30 W-hr/kg at a 2-hr discharge. The peak specific power was about 35 W/kg. Cell G-03-002 was operated for 79 cycles and 65 days and Cell G-02-002 for 43 cycles and 45 days. The series resistances of both cells were higher than expected. Gould has been operating identical cells in their Rolling Meadows, Ill. laboratory with reference electrodes, and they have identified the structure of the positive-electrode current collector as the major cause of these unexpectedly high resistances. Future designs of this type will incorporate improved positive-electrode current collectors.

In conclusion, Gould has developed a cell design that shows good potential and gives stable, reproducible performance. These are the criteria that are used to qualify baseline designs. The program at Gould can now move on to improved versions of this design with the confidence that these improvements can be objectively evaluated.

c. Performance of Eagle-Picher Cell 2B6

Eagle-Picher Cell 2B6 has been used in cell temperature studies, described later. Data generated in these studies are being used to investigate the capacity and energy output of the cell when it is operated on (1) the upper voltage plateau (to 1.5 V) (2) the upper plateau and transition region (to 1.25 V), and (3) the upper and lower plateaus (to 1.1 or 1.0 V). The utilization and energy output of the upper plateau and transition regions were compared with those of the lower plateau for the various cases of Table III-1. The effect of charge rate on capacity is also shown in Table III-1. Initially at 10-A charge and discharge currents (Case 1), about 60% of the energy was obtained from the upper plateau. After about 63 days

Table III-1. Effect of Charge Rate on Cell EP-2B6

	Case 1	Case 2	Case 3
Operating Time, days	9	72	84
Charge Current, A	10	10	5
Discharge Current, A	10	10	10
Capacity, A-hr			
Upper Plateau	57.9	32.5	57.5
Lower Plateau	50.4	42.1	35.8
Total	108.3	74.6	93.3
Energy, W-hr			
Upper Plateau	90.5	48.0	86.6
Lower Plateau	60.5	48.4	42.3
Total	151.0	96.4	128.9

(Case 2), at the same 10-A charge and discharge currents, the available energy had decreased by ∿36%, and the fraction of the energy obtained from the upper plateau decreased to ∿50%. One of the effects of the 5-A charge rate (Case 3) on the upper plateau appears to be to restore the contributions of both the energy and capacity to their initial values. However, on the lower plateau the contributions of both energy and capacity decreased by about 30%. The total effect of the low charge rate was to restore the capacity and energy of the cell to 85% of its initial value.

2. Performance of Cell in Air Atmosphere
(J. L. Hamilton, G. W. Redding, V. M. Kolba)

Testing is being continued to determine the effect of air on an operating cell (Eagle-Picher Cell 2B8); this test was conducted to assess cell performance in the event of leakage of a secondary container. Cycling at 13-A discharge and charge currents was resumed on cycle 157, after charge rate tests had been completed. After 32 such cycles, the capacity declined to ∿63 A-hr (∿26% decline) with a specific energy of 38 W-hr/kg. Next, the charge current was reduced to 10 A, while the discharge current remained at 13 A. Over the next 31 cycles, the capacity was ∿74 A-hr with a specific energy of ∿47.5 W-hr/kg. The charge current was then further reduced to 4 A, and, after three cycles, the capacity was ∿97.5 A-hr with a specific energy of ∿66 W-hr/kg. This specific energy is ∿85% of that initially obtained in cycle 11, and was achieved by reducing the charging current by a factor of ∿3. The energy obtained in these recent tests at 4 A compares very well with that obtained at 4 A during cycles 145-150.

After the above tests, cycling was continued in segments having 13-A or 4-A charges and 13-A discharges. After each series at the 13-A charge, the capacity declined from about 85 A-hr to about 72 A-hr. During the intermittent cycles at the 4-A charge rate, the capacity always reached about 97 A-hr.

The Cell EP-2B8 has now operated for more than 223 days and more than 354 cycles in an air environment. This cell, which is not hermetically sealed, has performed as well as identical cells operated inside an inert-atmosphere glove box.

3. Cell Heating and Cooling Experiments
(V. M. Kolba, J. L. Hamilton, G. W. Redding)

A preliminary experiment to measure temperature changes, described in ANL-76-81, p. 33, showed that temperature changes occur during cell cycling. A second experiment is now being conducted as described in ANL-77-17, p. 22. Using Eagle-Picher FeS_2 Cell 2B6, testing was done under 5, 10, 15, 20, and 25 A constant current charge and discharge conditions, and power tests were conducted at 25, 50, 75, and 100 A in the fully charged state. These experiments were conducted with equal charge and discharge currents. When the cell was not being cycled, its nominal temperature was 420°C.

The cell exhibited differing, but reproducible, temperature changes at the various current rates. At 10 A the maximum temperature occurred at the start of the discharge (end of charge cycle), and the minimum temperature occurred at the end of the upper voltage plateau, near the start of the transition region to the lower plateau. At 20 A the maximum temperature occurred at the end of the discharge cycle, with minimum temperature occurring at the end of the charge cycle. This effect may be due to the fact that the major portion of the discharge (∿90%) at this current is on the lower plateau. This result is corroborated by average discharge voltages of 1.39 V at 10 A and 1.16 V at 20 A. On this plateau, the entropic heat ($T\Delta S$) is additive to the ohmic heat (I^2R) on the discharge phase of the cycle. The cumulative

effect of testing at the various current levels in this quasi-adiabatic system is shown in Fig. III-1, where the cell maximum and minimum temperatures are plotted.

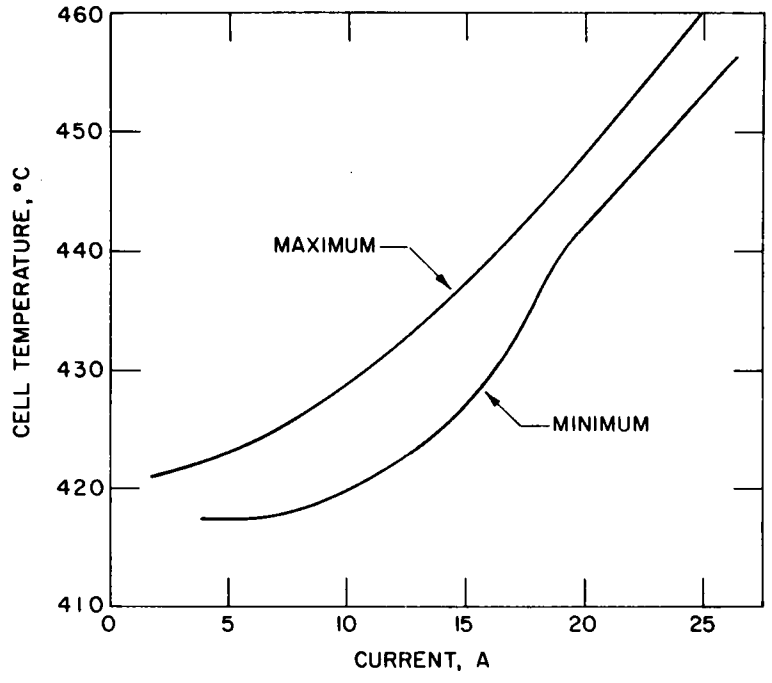

Fig. III-1. Temperature *vs.* Current for Cell EP-2B6 (cutoff voltages, 2.0 V charge and 1.0 V discharge; equal charge and discharge currents)

Discharge cutoff-voltage levels were also studied relative to cell temperature effects. The temperature spread was about the same (∿10.5°C) regardless of the cutoff voltage.

It was concluded from the above data that cooling may be required for the six-cell FeS_2 battery (described in Section III. A. 4 of this report) at high current rates. This situation may be ameliorated, however, if charging at lower rates reduces the temperature of the system. To evaluate this possibility, tests were conducted on the temperature effect of discharging and charging at mixed rates. The overall temperature swing at a 10-A discharge and a 5-A charge was about the same as that previously found with a 10-A discharge and a 10-A charge; however, when the 5-A charge was used, the nominal temperature was about 5°C lower than when the 10 A charge was used.

The effects of short-term (15 sec) and long-term (up to 5 min) high current pulses were also studied. The 15-sec tests were conducted on cycle 86. They showed a slight cooling effect (∿1°C) at 25 A,

very slight cooling at 50 A, and a very slight rise (<0.5°C) at 75 and 100 A. The peak specific power attained was about 38 W/kg at 75 A. With the cell essentially fully charged, a 5-min discharge at 50 A resulted in a temperature rise of about 1°C. This discharge was followed immediately by a 5-min discharge at 25 A, which resulted in a decrease in temperature of about 0.5°C. A subsequent 5-min discharge at 15 A further decreased the temperature by about 0.75°C.

During operation, an electric-vehicle battery will be subjected to a variety of charge-discharge conditions. The normal range of operating conditions for a cell have been investigated in the experiments described above. Only small temperature effects have been noted. Based on these studies, it appears that a simple temperature control and cooling system will be sufficient to keep the battery within the desired temperature range.

4. Battery Testing
(V. M. Kolba, G. W. Redding, J. L. Hamilton)

Cells have been tested separately in both parallel and series arrangements. When a sufficient number of cells become available, testing will be conducted in combined parallel-series arrangements. The cells tested in this program were individually monitored in the batteries for voltage, and charge or discharge was terminated when one individual cell of the battery configuration reached its voltage limit. Descriptions of the batteries are given in Table III-2 along with lifetime status. A summary of battery performance data is given in Appendix A.

Table III-2. Description of Batteries

	Battery No.		
	B7-S	B9-S	B10-S
Cell Type	FeS (thick)	FeS (thin)	FeS_2 (thick)
Cell No.	EP-1B4, -1B6	EP-1A7, -1A8	EP-I-5-1, -3, -4, -5, -7, -8
Capacity, A-hr	149	69	156
Total Operating Time			
Days	>295	62	>23
Cycles	>472	164	>19
Status	Operating	Terminated	Operating

a. Two-Cell Battery Test B7-S

During this period, cycling of Eagle-Picher FeS Cells 1B4 and 1B6 in series (designated Battery B7-S) was continued. Tests were performed to determine the effect of intermediate shallow cycles on subsequent deep cycling in the battery. After more than 115 cycles under

the cycling mode, described in ANL-77-17, p. 24, a trend of decreasing performance (∿10% at the 5-hr rate) was noted. This trend resulted from insufficient equalization charge time. After several cycles employing 10-hr equalization times, the cells were brought into balance, and the performance at the 5- and 10-hr rates was approximately the same as that obtained previously. The specific energy of the battery is now about 33 W-hr/kg at the 5-hr rate. The battery has operated for more than 295 days and 472 cycles. Cell EP-1B4 in this battery has operated for more than 344 days and 516 cycles.

b. Two-Cell Battery Test B9-S

During this period, testing of Eagle-Picher FeS thin Cells EP-1A7 and 1A8 in series (designated Battery B-9S) was voluntarily terminated to permit installation and check-out of equalization equipment for the six-cell battery tests. The cells had been tested on the new energy storage cycle, as described in ANL-77-17, p. 24, using bulk charging only. The achievable capacity and energy continually declined under this regime. One cell (1A8) limited the discharge while the other cell (1A7) limited the charge. The capacity under this mode declined about 50% in 125 total cycles. The coulombic efficiency remained high, as did the energy efficiency. During the checkout of the new equipment, Cell 1A8 was inadvertently over-charged. Cell 1A7 was individually tested and yielded a capacity of 53 A-hr with a specific energy of ∿49 W-hr/kg at the 5-hr rate. This is slightly greater than the specific energy of 45 W-hr/kg that was achieved by the battery early in its life. Cell 1A8 has been submitted to the Materials Group for postoperative analysis (see Section IV. A. 9).

c. Six-Cell Battery Test B10-S

Lithium/iron sulfide cells have been successfully tested as batteries in heated test chambers. The next phase of the program is to demonstrate the operation of a battery in a portable, insulated case. An insulated case, with reflective foil insulation in a vacuum annulus in all areas except for the front access plug, was obtained from Linde* during the last reporting period. To permit use of this case for testing of the six cells, design modifications were made to the front plug and internal support structures were designed. Provisions were made for current leads, voltage leads, equalization leads, heater power leads, thermocouples, and gas purge lines as well as for orientation, support, and clamping of the cells. The assembled unit is shown in Fig. III-2. Figure III-3 is a view of the cell package with the voltage, equalization, and cell interconnection leads.

The six Eagle-Picher Type B FeS_2 (two-plateau) cells (I-5-1, -3, -4, -5, -7, and -8) were assembled using mica sheets for electrical insulation, and were connected in series for test purposes. This assembly was successfully started up and conditioned in a test chamber. Discharge and charge currents of 7.5 A were used for the initial break-in cycles. The performance of the six-cell battery during the first four cycles is given in Table III-3.

*A Division of the Union Carbide Corp.

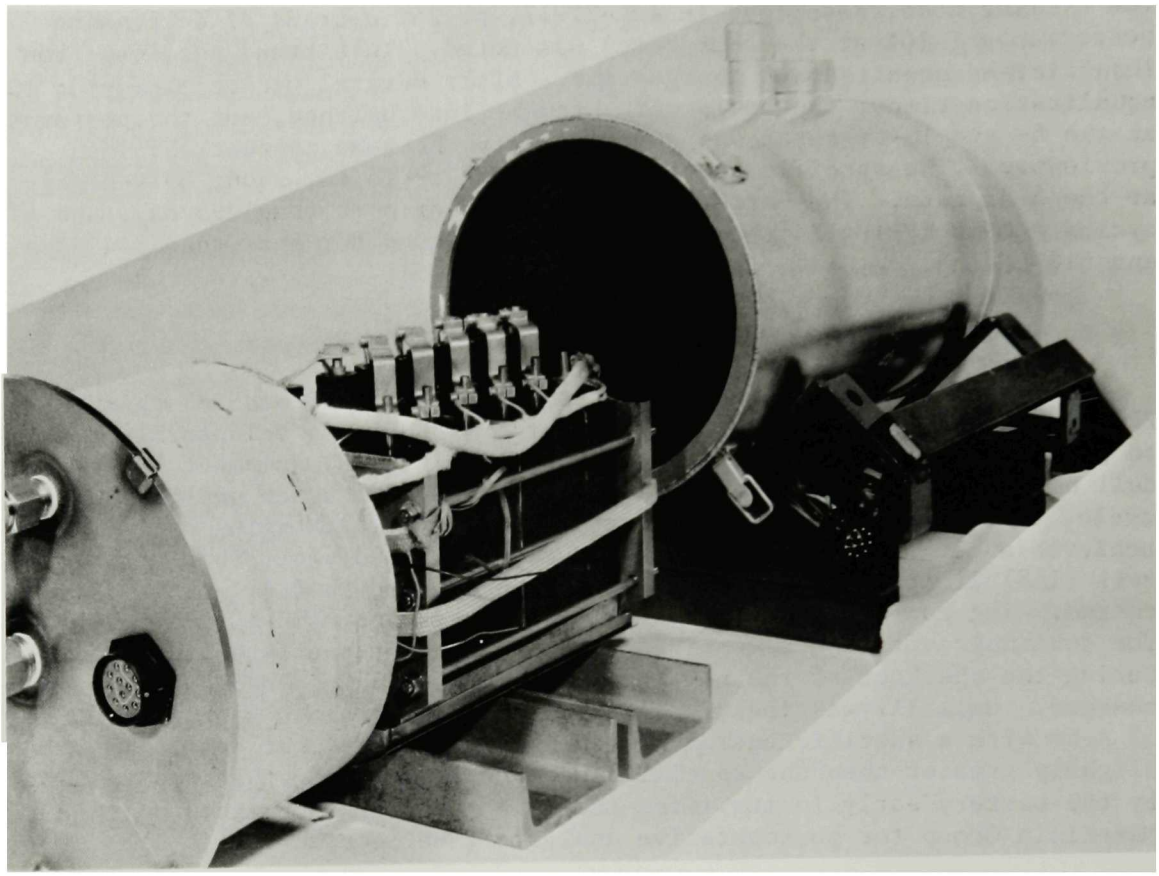

Fig. III-2. Assembled Six-Cell Battery

Table III-3. First ANL Test of Six-Cell Lithium/Metal Sulfide Battery

	Discharge No.			
	1	2	3	4
Current, A	7.5	7.5	7.5	7.5
Ave. Voltage, V	8.6	8.99	8.85	8.83
Capacity, A-hr	89.7	103.1	119.7	122.7
Energy, W-hr	771.5	927.3	1059.1	1083.4
Specific Energy, W-hr/kg	62.2	74.8	85.4	87.4
Coulombic Efficiency, %	>99.0	96.8	99.5	>99.0
Energy Efficiency, %	83.0	85.0	88.0	89.0

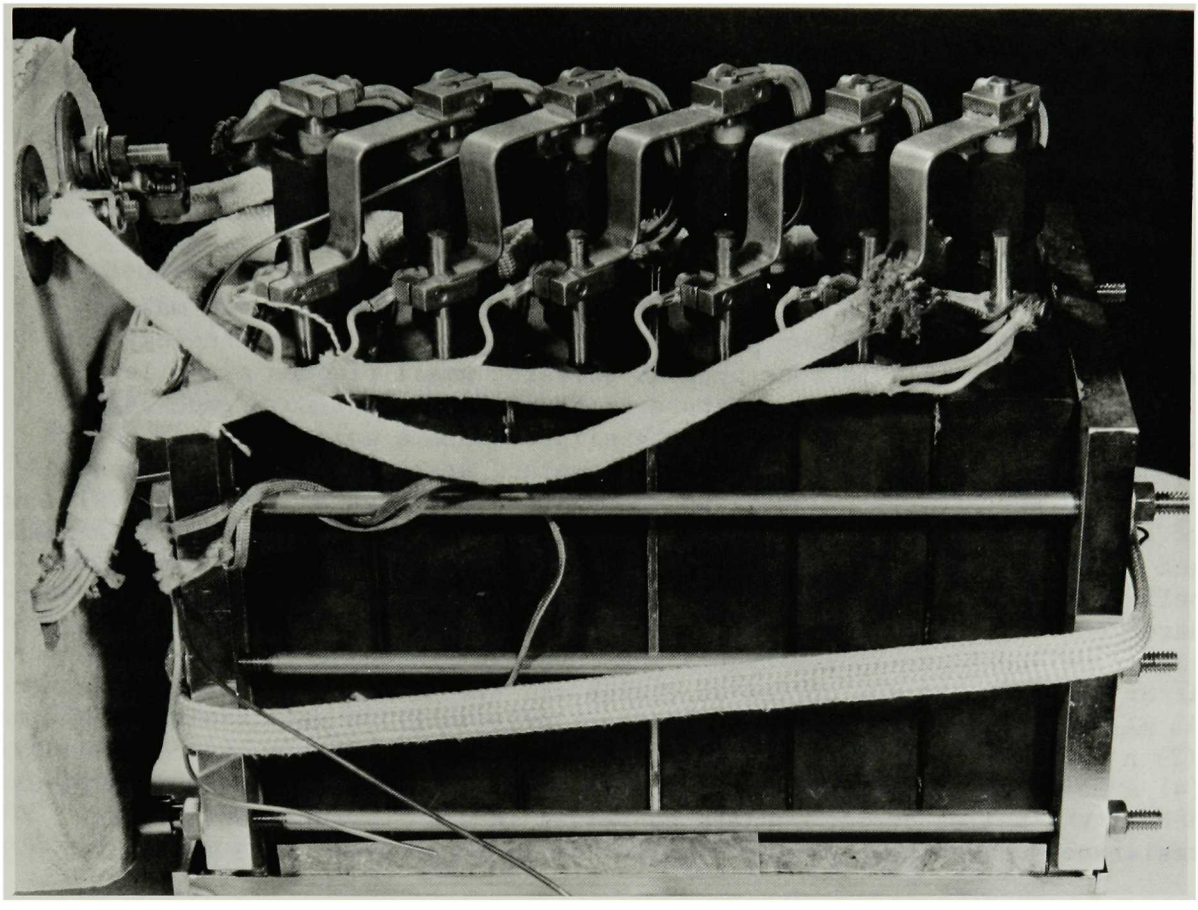

Fig. III-3. Cell Configuration of Six-Cell Battery

After cycling in the test chamber, the cells were assembled as shown in Fig. III-3, and placed in a vacuum insulated housing (Fig. III-2); performance and temperature measurements were then made. This was our first attempt to place cells in an insulated container. Many of the anticipated problems were confirmed, and new ones were revealed by this exercise. Some of these problems are the need for the following: weight reduction, higher purity atmosphere, better thermal and electrical insulation, and better intercell connections (probably brazed).

The case provided good insulation: with a battery temperature of 435°C, the external temperature of the case was <25°C. At the interface of the front of the case with the insulated plug, the external case temperature was about 45-50°C. The heat loss was less than anticipated with the addition of the modified plug, leads, etc. The power necessary to maintain the temperature of the battery at ∿435°C was 57-60 W, which is about 23% more than that indicated by previous data from tests using a plug with no penetrations.

There was a 15°C temperature difference from the front face to the center of the cell stack, and a further 8°C difference to the back face of the cell stack. There was a 2°C difference from cell top to bottom.

Because the multi-pin connectors and the other interfaces with the plug were not leak-tight, the battery was purged continuously with argon. An analysis of the atmosphere in the case with the battery at its normal operating temperature indicated 0.1% O_2; 0.8% H_2O; 5% CO_2; 5% other (including hydrocarbons), 22% N_2; and balance argon.

5. Pellet Cell Development
(R. Thompson, P. F. Eshman)

A new type of cell construction is being developed to make possible the application of high-speed electrode pressing technology for any size cell. This is done by cold-pressing small plaques or pellets (2.5 x 2.5 x 0.5 cm) from a mixture of 46 wt % FeS, 16% Cu_2S, and 38% electrolyte. These pellets are then slipped into a welded grid structure of metal channels. Advantages of this method are: (1) small, high-speed automated presses can be utilized in making electrodes of any size; (2) control of the distribution, thickness and density of the active material is enhanced; and (3) current collection is probably improved. Thus far, two positive pellet-grid electrodes and one pair of negative pellet-grid half electrodes have been fabricated. One FeS cell (PC-1-01) using a pellet-grid positive electrode and Eagle-Picher type B negative electrodes is in operation. After 102 days and 137 cycles at charge and discharge current densities of 44 mA/cm^2, this cell is consistently achieving: (1) a utilization of 67%; (2) a coulombic efficiency of > 99%; (3) a watt-hour efficiency of 85%; and (4) a measured internal resistance of 5-7 mΩ (15-sec interruption: $\Delta V/I$). Hence, the pellet design appears to result in significantly lower cell resistances than those of the baseline cells (typically, 8-10 mΩ).

B. Battery Charging and Control Systems

1. Charging Systems for Li-Al/FeS_2 Electric-Vehicle Battery
(F. Hornstra)

Proposals were received from TRW and Gulton, Inc. to complete a cost and design study for a full-scale battery charging system complete with cell equalizers for the Li-Al/FeS_2 electric-vehicle battery. The proposals have been reviewed, a selection has been made, and a procurement package is being prepared.

2. Electronic Development
(F. Hornstra, W. W. Lark, J. M. Paul*)

A six-cell monitor and equalizer control system that has been placed in operation on the six-cell Li-Al/FeS_2 battery (B10-S) is performing well.

The detailed design of a 100-A cell and battery cycler was completed, and construction has started. This device will handle up to four Li-Al/FeS_2 cells connected in series. The cycler has capabilities

*ANL Electronics Division

for constant-power discharge and current-limited, constant-voltage charge. Other features include timers for length of discharge, open-circuit time after charge and open-circuit time after discharge. The cycler is being constructed from a commercially available regulated power supply.

One of the 25-A "mini-cyclers" has been modified to allow cell charging in either a constant-current or a constant-voltage mode. This modification allows cell charging to be completed at a constant voltage, which should increase the cell capacity over that achieved when charging is terminated in the constant-current mode. A modification package is being designed to allow retrofitting of other mini-cyclers as required.

C. Cell Development and Engineering
(H. Shimotake)

The effort in this part of the program is directed toward the development and testing of Li-Al/FeS_x cells having improved performance and cycle life with low cost. Technical advances resulting from this effort are incorporated into the cells that are fabricated by industrial firms. The work is concentrated on the development of cells that are particularly adaptable to electric-vehicle application, with emphasis on high specific energy at the 2- and 4-hr discharge rates. Specific energies over 100 W-hr/kg at the 4-hr rate were obtained with cells using an advanced separator/retainer, such as Y_2O_3 felt. Efforts are also under way to use powder separators in compact engineering cells. An assembly of "upper-plateau" FeS_2 cells in air was initiated during this quarter. A summary of performance results of the test cells is presented in Appendix A.

1. Cell Performance and Lifetime Improvement

a. Uncharged Cells with Hot-Pressed FeS_2 Electrodes
(L. G. Bartholme, E. Voss,* H. Shimotake)

Two upper-plateau FeS_2 cells, VB-1 and VB-2, were built with Li_2FeS_2 (a discharge product of an upper-plateau cell, commonly known as "X-phase") as the starting material in the positive electrode. This material is relatively unaffected by air or moisture. Therefore, a positive electrode of this type with an aluminum plaque can be assembled in air to form an uncharged cell; this technique has potential as a method for fabricating an upper-plateau cell. Cell VB-1 was built partially in air and partially in a helium atmosphere, and VB-2 was fabricated completely in air. Potassium chloride, instead of LiCl-KCl eutectic, was used as the binder for the positive plaque and for pretreatment of the BN fabric separator. The performance of these cells (utilization, coulombic efficiency, cell voltage, etc.) was equivalent to that of similar cells built in a helium atmosphere. Scale-up of cells fabricated in this method is under way.

Four uncharged, upper-plateau FeS_2 cells (R-25, -26, -27, and -29) were built. In this series of cells, the amounts of excess lithium and aluminum in the negative electrodes varied from 0 to +50%. The higher

*Industrial Participant from Varta Batteries A. G., Germany.

lithium and aluminum concentrations yielded better FeS_2 utilization; this improvement was attributed to the additional current collection provided by the excess lithium and aluminum. In some cells, the excess lithium in the negative electrode was added in the form of sheets of thin lithium foil that had been pressed between layers of aluminum foil. The foils are less subject to contamination by gaseous impurities than Li-Al powder.

b. Carbon-Bonded Metal Sulfide Electrodes
(T. D. Kaun, W. A. Kremsner, F. J. Martino, W. Borger*)

Cell CB-1, constructed as an unsealed, charged cell, was designed to test a positive electrode of carbon-bonded chalcopyrite ($CuFeS_2$) with hot-pressed pyrometallurgically prepared Li-Al negative electrodes. After 736 cycles and 427 days, cell capacity declined only 15% from its typically high value of 67 A-hr at the 5-hr discharge rate (12.5 A, 65 mA/cm^2). The discharge and charge cutoff voltages have been maintained at 0.9 V and 1.75 V (IR included), respectively. Cell resistance has been stable at approximately 13 mΩ, and the coulombic efficiency has remained at ∿93%.

One of the significant findings in recent carbon-bonded electrode development is the stability of the carbon structure during operation of the uncharged electrode. A photomicrograph of Cell TK-13 exhibited "carbon rings" after 50 cycles, thereby suggesting the existence of a tenacious carbon current-collecting matrix. For similar electrodes prepared with furfural alcohol resin,† tests have shown carbon powder filler to provide better overall electrode performance than graphite powder filler. Although graphite slightly reduced the electrode resistance, gas absorption was believed to lower the electrode capacity. Promising results were obtained in the development of "electrolyte-sponged" electrodes for reduction of excess electrolyte. One such cell, TK-16, an uncharged FeS cell fabricated in air, used positive and negative electrodes containing 5 vol % Y_2O_3 to aid electrode wetting. Two prewetted electrodes separated by a prewetted BN cloth disk were assembled with the excess electrolyte drained off. This type of electrode resulted in a reduction of about 30% in the electrolyte content. At present, the cell is operating with stable capacity.

Cells KK-5, -6, -7, and -9 are sealed prismatic cells; their physical characteristics appear in Appendix A. Cell KK-5, an uncharged FeS cell with Cu_2S additive, has completed 460 cycles in 333 days with a discharge cutoff voltage of 1.0 V. Its 90 A-hr capacity had diminished by <10% when it attained a lifetime goal of 400 cycles with 99+% coulombic efficiency. Its recent operation has been hampered by a short circuit in the feedthrough. After dismantling the feedthrough, 99.5% coulombic efficiency was restored. The cell resistance remains low at 4.5 mΩ. A new design of a molybdenum current collector with a welded connection has reduced the resistance of the KK-series FeS_2 cells from 6-8 mΩ to 4.5 mΩ, as demonstrated by Cell KK-7. The welded connection, which uses

*Industrial Participant from Varta Batteries A. G., Germany.

†A product of Quaker Oats.

a quartered molybdenum rod design, is located inside the electrode rather than on a tab. Cells KK-9 and EP-2B5 enabled a comparison to be made between carbon-bonded and cold-pressed FeS_2 electrodes. These types of electrodes have shown similar performance, but the carbon-bonded electrode did not require break-in cycles to attain its full capacity whereas the cold-pressed electrode did.

c. Charged Cells with Hot-Pressed FeS_2 Electrodes
(F. J. Martino)

To characterize charged, upper-plateau FeS_2 cells with a compact cell design, a series of tests was performed on cells having hot-pressed, charged electrodes and an advanced separator/retainer material such as Y_2O_3 felt. Lithium-aluminum alloy containing 55 at. % Li was used in the negative electrode.

Two such cells, M-1 and M-2, have been built and placed in operation. Both cells are prismatic (13 x 13 cm). Each cell has a positive electrode consisting of a hot-pressed mixture of FeS_2-10 mol % CoS_2 and 60 vol % LiCl-KCl eutectic. Molybdenum honeycomb current collectors were welded to a 0.64 cm (1/4 in.) dia molybdenum terminal, as shown in Fig. III-4. The positive electrode was placed between two negative electrodes consisting of a hot-pressed mixture of Li-Al (55 at. % Li) and 30 vol % LiCl-KCl eutectic in iron honeycomb trays. A separator/retainer consisting of double layers of Y_2O_3 felt (94% porosity, 4 mm thickness) was placed between the electrodes. The major difference between the two cells was in the Cell M-2 housing. In Cell M-2 the negative electrode current-collector trays were an intrinsic part of the housing, thus making the cell considerably lighter than Cell M-1.

Although Cell M-1 developed a short circuit after 17 cycles and 17 days, it showed unusually good upper-plateau performance (see Fig. III-5), with a capacity of 144 A-hr and a specific energy of 98 W-hr/kg at a 25-A discharge rate (current density, 92 mA/cm^2). This corresponds to an upper-plateau utilization of 98%. The contribution of the welded molybdenum connection to improved performance was reflected in the low cell resistance of 2.7 to 4.8 mΩ. The high average discharge voltage (1.60 V) demonstrates the beneficial effect of the lithium-rich Li-Al alloy.

The above performance was essentially reproduced with Cell M-2. Because of the modified cell design that resulted in a weight reduction of 360 g, the specific energy of Cell M-2 was increased by 10% over that of Cell M-1, from 98 to 110 W-hr/kg at the 25-A discharge rate. This cell has accumulated 15 cycles and 14 days of operation to date. A distribution of the component weights of these two cells is listed in Table III-4.

2. Large-Scale Cell
(F. J. Martino, T. D. Kaun)

Cell SS-1, a 25 x 35 cm compact cell containing a charged, carbon-bonded FeS-Cu_2S positive electrode and negative electrodes of pyrometallurgically prepared Li-Al in iron Retimet,* has been sealed and put

*A porous metallic material produced by Dunlop, Ltd., Coventry, England.

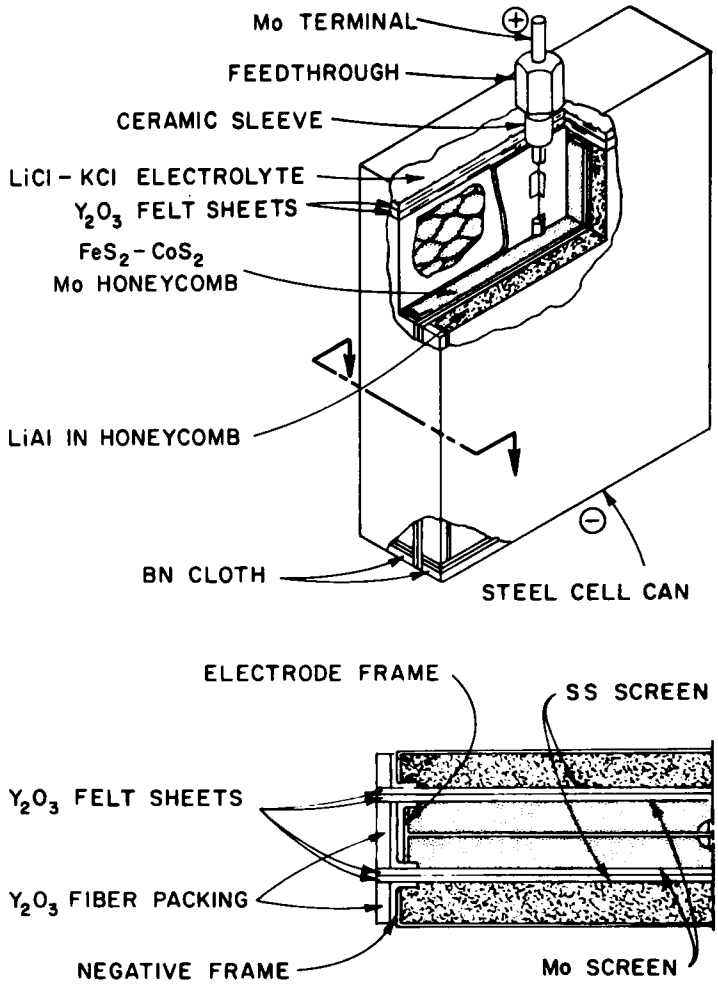

Fig. III-4. Schematic Diagram of Cell M-1

back into operation. It has accumulated 195 cycles and 180 days of operation with capacities in the range of 280 to 450 A-hr while discharging at currents as high as 80 A (50 mA/cm^2). Although the coulombic efficiency generally remained >98%, the cell capacity declined by about 30%, from an earlier typical value of 400 A-hr to the present typical value of 280 A-hr. The cell resistance was doubled, to 3 mΩ, by moving the positive electrode voltage terminal farther away from the electrode during the sealing procedure.

During operation of the cell, the surface of the LiCl-KCl electrolyte* solidified around the positive electrode terminal. It was not possible to remelt the salt by raising the temperature from 450 to 490°C. An analysis of a salt sample revealed that it was no longer a eutectic composition and that the KCl content was reduced by nearly one half. The solid layer was dissolved by adding fresh electrolyte spiked with ∿5 wt % KCl.

*Procured from the Lithium Corporation of America, Bessemer City, N.C.

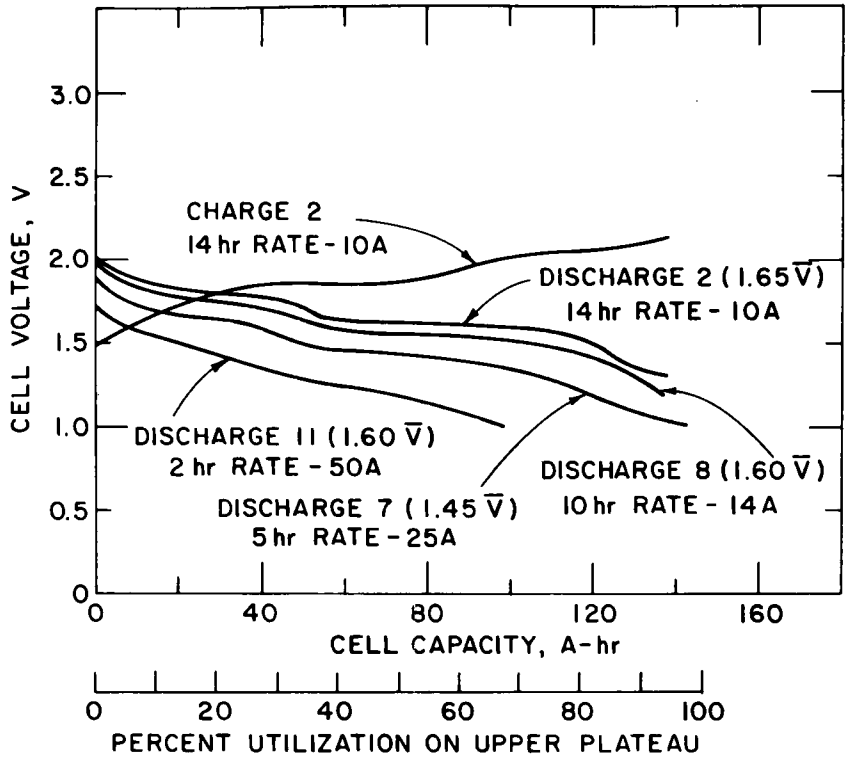

Fig. III-5. Voltage *vs.* Cell Capacity Curves of Cell M-1

Table III-4. Component Weights of Upper-Plateau Cells M-1 and M-2

	Cell Weight, g	
	M-1	M-2
Positive Active Material	329	327
Negative Active Material	218	219
Positive Current Collector[a]	210	206
Negative Current Collector	192	244[b]
Separator and Retainer[a]	86	55
Electrolyte[a]	583	536
Cell Can[a]	381	188
Feedthrough	157	157
Total	2,160	1800

[a]Weight sensitive components.

[b]Includes 132 g also serving as cell can.

3. Electrode Development

a. Li-Al Alloy Negative Electrodes with Additives
(F. J. Martino, H. Shimotake)

Engineering-size cells (13 x 13 cm) are being operated to evaluate the effects of the addition of a third metal to the Li-Al alloy (FM series cells). These cells consist of a commercially fabricated (Eagle-Picher), cold-pressed FeS-Cu_2S positive electrode (70 A-hr theoretical capacity) placed between two negative electrodes in which the three-metal alloy has been loaded into iron Retimet current collectors. The charge-discharge current for these test cells, the IR-included cutoff voltages, and the operating temperature are being held constant at 8.0 A, 1.00-1.70 V, and 450°C, respectively.

The test of Cell FM-1, which had negative electrodes of Li-Al-4 wt % In (85 A-hr theoretical capacity), was terminated after 318 cycles and 159 days. An apparent short circuit had developed, as indicated by a decline in the coulombic efficiency from 100 to about 86%. As a result, the cell capacity declined ∿30%, from a typically high value of 55 to 39-A hr. Cell FM-1 is currently undergoing postoperative analysis. Cell FM-2, which had negative electrodes of Li-Al-8 wt % Ca (90 A-hr theoretical capacity), was terminated after 74 days and 126 cycles. The results of this cell were reported previously (ANL-77-17, p. 30). Cell FM-3, still in operation after 186 cycles and 109 days, has negative electrodes of Li-Al-8 wt % Sn (86 A-hr theoretical capacity). The capacity has declined about 10%, from 57 to 50 A-hr; similarly, the coulombic effficiency has declined from about 100 to 89%. As indicated in Fig. III-6, the capacity of Cell FM-3 is significantly greater than the capacity of either Cell FM-1 or Cell FM-2.

In addition to the above cells, a new series of cells is being fabricated to test the more promising three-metal alloys against commercially fabricated (Eagle-Picher) FeS_2-CoS_2 positive electrodes.

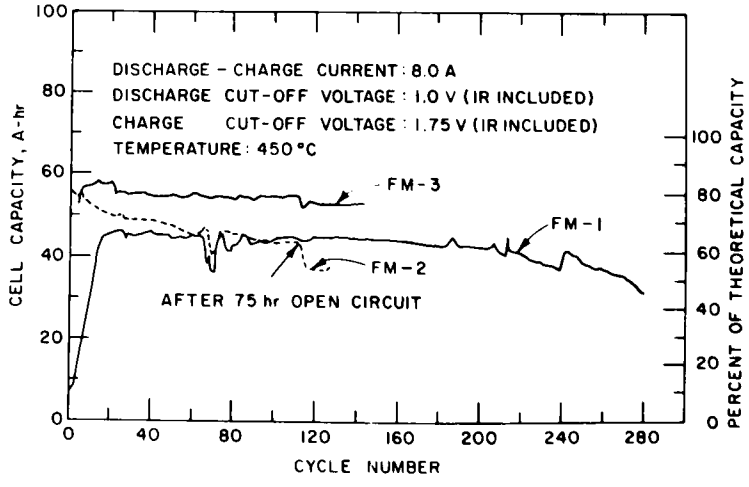

Fig. III-6. Capacities of Cells FM-1, FM-2, and FM-3

b. Electrodes with Advanced Separators
(T. W. Olszanski, H. Shimotake)

Five cells, (TO-2, -3, -4, -5, -6) each of approximately 120 A-hr capacity with compact designs and nonwoven cloth separators, have been built and tested. (See Appendix A for individual performance data.) These test cells have shown that the Y_2O_3 and BN felt separator/retainers have many advantages over the BN and ZrO_2 cloth separator/retainers presently in use in full-scale engineering cells. These advantages include: (1) achievement of a >60% weight savings in separator material; (2) attainment of lower internal resistances; (3) ease of wettability and minimal outgassing, therefore permitting more immediate and uniform utilization of electrodes; (4) a significant cost savings in separator materials; (5) an effective particle retainer and insulator contained in one; and (6) a reduction in the amount of electrolyte retained in the separator.

A compact engineering-scale cell utilizing a Y_2O_3 powder separator (ANL-77-17, p. 35) has been built, and is presently in operation. All components were pressed together in two hot-pressing operations. The final product was placed in a can and sealed. The electrolyte content is less than 300 g (20 wt % of cell weight), which corresponds to a weight reduction of approximately 200 g from a similar cell. Internal resistance at start-up was relatively low, despite the low loading of electrolyte.

IV. TECHNOLOGY DEVELOPMENT
(R. K. Steunenberg)

A. Materials Development
(J. E. Battles)

Efforts in the materials program are directed toward the development of various cell components (electrical feedthroughs, electrode separators, current collectors, cell hardware, etc.), testing and evaluation of cell materials (corrosion, wettability, etc.), and postoperative examination of cells to evaluate the behavior of the electrodes and the construction materials.

1. Electrical Feedthrough
(K. M. Myles and J. L. Settle)

The corrosive environment within Li-Al/LiCl-KCl/FeS_x cells precludes the ready adaptation of most commercially available electrical feedthroughs. The few that are compatible with the cell environment do not meet the technical goals of weight, cost, and leak-tightness. Perhaps the best long-term solution would involve a brazed feedthrough, but to date no reliable feedthrough has been found, although some significant progress has been made. The ANL crimp-type, mechanical feedthrough has been sufficiently refined to offer an alternative to the brazed feedthrough in every respect other than the most stringent size limitations.

Throughout the past several years exploratory programs have been undertaken by commercial feedthrough manufacturers. Most of these efforts attempted to protect the metallic braze interface from corrosive attack; however, in every case, the resultant feedthroughs exhibited premature failures in simulated cell tests. Thus, the likelihood of finding a suitably protected metallic braze was concluded to be poor.

A brazed feedthrough is only considered possible through the use of a braze material that is corrosion resistant. Accordingly, Coors Porcelain was contracted to produce a nonmetallic braze for Y_2O_3. Yttria was selected because of the intrinsic corrosion resistance of the oxide. In addition, this oxide has properties which suggest that a braze may be more adherent to it than to alternative oxides. Several brazes have been sufficiently developed to warrant testing of the compatibility of Y_2O_3 braze combination (molybdenum sheets bonded to Y_2O_3-braze test rings). The results of these compatibility tests indicate that the Y_2O_3 braze combination is able to withstand the cell environment. Some difficulty was experienced in bonding the molybdenum onto the Y_2O_3 because of differences in thermal expansion between the two materials. This is a familiar problem in bonding metals to ceramics, and Coors believes that a solution can be found through proper design.

As described in the previous report (ANL-77-17, p. 32), several significant modifications have been incorporated into the Conax mechanical feedthrough that have resulted in a design that better meets the needs of the battery program. The ANL crimp-type feedthrough optimizes the design in such a way as to reduce the overall weight of a feedthrough for a 1/4-in. (6.35 mm) conductor to only 46 g and the potential cost to $1.14. A press has been designed for the crimping of feedthroughs while attached to assembled

cells; it is near completion in the machine shop. Most recently, a die and ram combination was designed that forms a precompacted pellet of the BN sealant powder. The pellet can be handled in the glove-box considerably easier than the loose powder that was used previously. Drawings for the feedthrough, crimping press, and compaction die set are being sent to Eagle-Picher for use in future cells and to Atomics International for evaluation. Operational instructions and specifications will also be sent as soon as sufficient operating experience is accummulated. The crimp-type feedthroughs will probably be used on some of the Mark-I electric-vehicle cells.

2. Current Collector Development
(K. M. Myles)

Cost projections of the LiAl/LiCl-KCl/FeS_2 cells indicate that the current collector for the FeS_2 electrode is one of the more expensive components. A program is under way to examine the long-term costs of various current-collector designs, to determine the quantity and distribution of current collector required, to develop alternative materials to molybdenum, and to find methods of fabricating current-collector assemblies. The results of this effort are still preliminary; however, sufficient information has been accumulated to identify the areas where additional data are required.

The following current-collector designs were studied to determine their costs: flat-sheet molybdenum, honeycomb molybdenum, and molybdenum porous metal. The results indicate that the honeycomb is the most expensive collector design. The honeycomb design would meet only our earliest (1981) cost goals, whereas the porous metal and flat-sheets designs would meet our intermediate (1985) cost goals. None of the designs would meet our long-range (1990) goals. One possible solution to meeting our long-range cost goals is the development of a compatible coating for iron current collectors. An effort to locate competent outside organizations to develop such coatings is under way, and several research proposals have been received and are being reviewed.

The development of a method of bonding molybdenum current-collector components is one of our more immediate needs. Molybdenum recrystallizes into a brittle form upon conventional welding; to circumvent this problem, a program is under way at Chemetal to investigate the possibility of forming a bond by vapor deposition of molybdenum onto the collector assembly. Amax Specialty Metals is looking into diffusion bonding and high-frequency, tungsten inert-gas (TIG) welding for the same purpose. Both of these programs are just beginning, and no significant results have been produced as yet.

3. Electrode Separator Development
(J. P. Mathers and C. W. Boquist)

Paper, felt, and powder separators are being developed as alternatives to the BN fabric which is currently used as the electrode separator in Li-Al/LiCl-KCl/FeS_x cells. These candidate separators are expected to be considerably less expensive than BN fabric and to provide more effective retention of the active materials in the electrodes.

Work on the development of an all-powder electrode separator was continued this past quarter with the construction and operation of Cell SC-14. This cell was assembled in the uncharged state using a hot-pressed mixture of Li_2S, Fe, and LiCl-KCl for the positive electrode and a pressed plaque of Al wire for the negative electrode. The cell was cylindrical (7.6 cm dia) with horizontal electrodes. The positive electrode, current collector, and the upper and lower electrode separators were assembled in a single hot-pressing operation using electrolyte (LiCl-KCl) as the binder (Fig. IV-1, top). The sides of the electrodes were insulated from the cell housing by separator powder that was packed into place. A schematic diagram of the assembled cell is shown in Fig. IV-1, bottom.

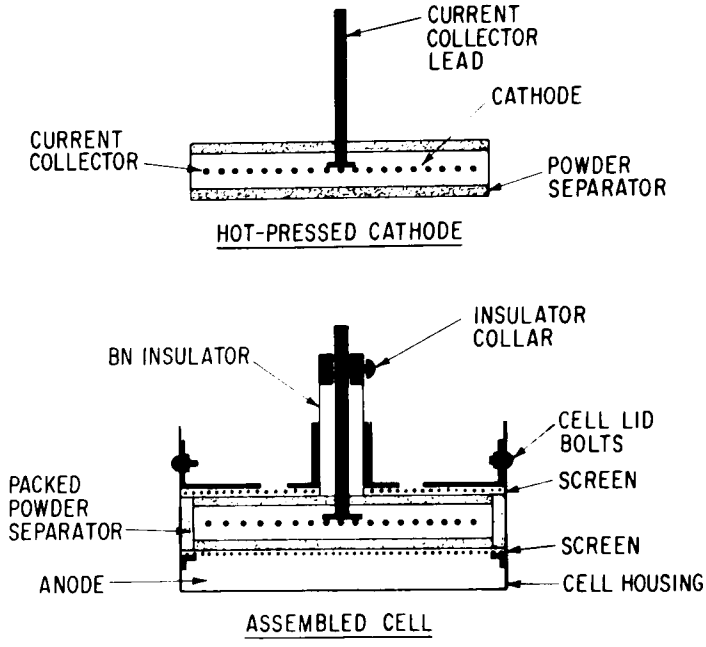

Fig. IV-1. Separator Test Cell SC-14

The separator consisted of 70 wt % coarse Y_2O_3 powder (150-250 μm) and 30 wt % fine Y_2O_3 powder (1-10 μm). Coarse powder was selected because it does not migrate into the positive electrode or through the 325-mesh screen used to cover the negative electrode. The fine Y_2O_3 particles were expected to occupy the pores between the larger Y_2O_3 particles and limit the migration of fine electrode particles through the separator. The thickness of each separator layer after hot-pressing was 2 mm.

The cell was cycled continuously at a current density of 60 mA/cm^2 for over 1000 hr (78 cycles) before its operation was voluntarily terminated. The electrical performance of this cell was excellent; the coulombic efficiency remained near 100% with a utilization of 40-50% throughout its operation.

Post-test examination of the separator revealed the presence of a few fine particles from the positive electrode adjacent to that electrode, but the remaining thickness of the separator (~90%) was free of electrode particles. The separator maintained a uniform thickness around the positive electrode, and did not contain any large voids.

These results are very encouraging. They indicate that it may be possible to eliminate the positive frame and screen assembly with powder separators, thus eliminating the corrosion problem associated with this component of FeS_2 cells.

Work is currently in progress to evaluate separator powders that have a lower cost potential than Y_2O_3 and to evaluate the performance of all-powder separators in vertical, prismatic cells. Work is also in progress to determine more fully the ability of BN fabric to retain the active materials of a cell within the electrodes.

4. Ceramic Materials Development
(W. D. Tuohig and J. T. Dusek)*

The performance of battery separators is known to be governed by pore volume fraction, size and size distribution, and connectivity of the separator material.[3,4] These same characteristics determine the ease with which a fluid may be made to flow through a porous material under a pressure gradient. Fluid conductivity, or permeability, can be regarded as a physical property of a porous solid, as first demonostrated by *Darcy* in 1856.[5] Darcy found that the flux of a fluid through a body is proportional to the applied pressure gradient according to the following equation:

$$q = \frac{K}{\mu} \frac{dP}{dx}$$

where q is the flux of fluid, μ is the viscosity of fluid, dP/dx is the pressure gradient, and K is a constant for the material.

A schematic diagram of the experimental apparatus constructed to measure permeability is shown in Fig. IV-2. It is similar to that used by Eusner and Shapland,[6] and adopted by the American Society for Testing and Materials.[7] Two speciment holders have been placed in parallel to permit direct comparison under identical flow conditions. A manometer is used to measure the differential pressure across the specimen. By-pass flow around the specimen is prevented by a high-compliance rubber gasket that is cast directly onto the specimen.

Preliminary measurements have been made on specimens that were prepared by incorporating volatile organic materials with Y_2O_3 powder prior to pressing. Upon heating to elevated temperatures, the organic additives evaporate, thus leaving vacant the volume which they had occupied in the powder compact. The remaining oxide powder particles bond together by normal sintering processes to form a highly porous solid. Figure IV-3 shows scanning-electron microscope photographs of two specimens prepared in this manner. The material in Fig. IV-3a was fabricated from as-received powder, whereas

*ANL Materials Science Division.

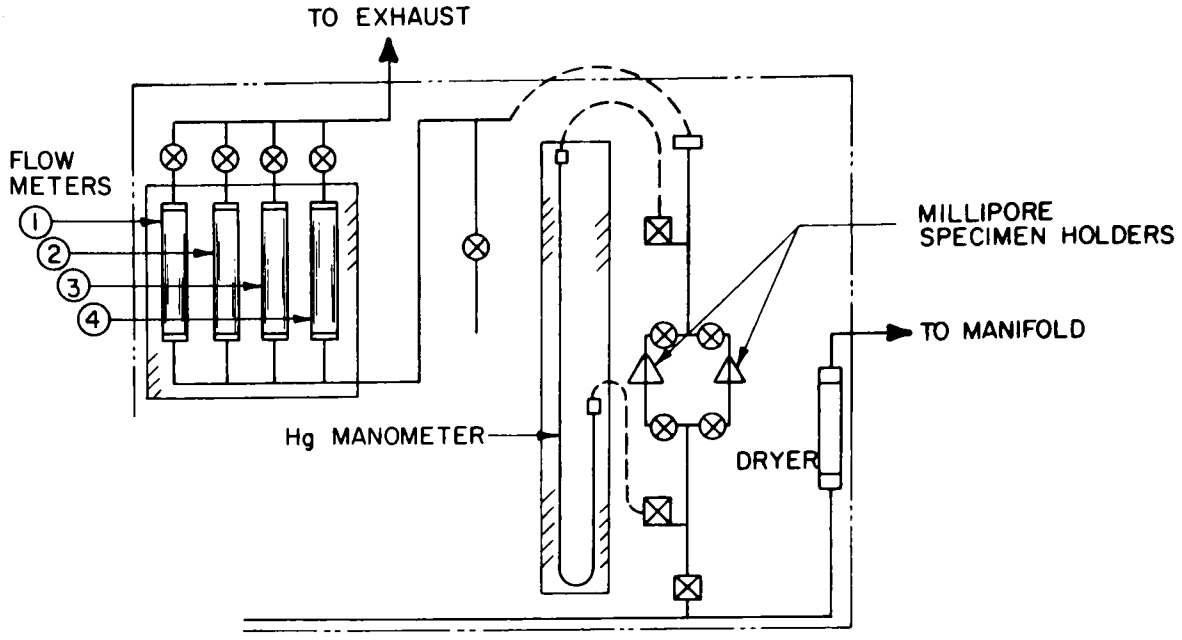

Fig. IV-2. Experimental Apparatus for Determining the Permeability of Interelectrode Separators.

the material in Fig. IV-3b was made from powder that had been calcined at high temperatures. Specimen 3a has a total porosity of 41%, and exhibits a broad range of pore "sizes" with clusters of high-density material. Specimen 3B is more homogeneous and has a slightly lower porosity (36%). The permeability of Specimen 3a is 7.4 millidarcies, whereas that of Specimen 3b is 11.4 millidarcies. Thus, although Specimen 3b contains less apparent porosity, its resistance to flow is nearly half that of Specimen 3a. Table IV-1 compares porosity with permeability for common porous materials.

Additional flowmeters are currently being added to the permeability apparatus to improve the accuracy of measurements over a broader range of flow conditions. These data will allow quantitative comparison of both flexible and rigid separator candidates, and will serve as a basis for predicting separator performance.

A commercial device* is being used to produce preformed foam by mixing aqueous solutions of organic materials and air under pressure. The consistency of the foam is determined by the ratio of liquid to air. A typical foam has a density of about 0.05 g/cm^3. This preformed foam is then mixed with an aqueous slip of Y_2O_3 powder in dilute nitric acid. As discussed previously (ANL-77-17, p. 35) the acid causes the structure to solidify into a rigid form that retains its foamed structure. The process is completed by firing at elevated temperatures.

*Model OT10-1A foam generator, the Mearl Corp., Roselle Park, NJ.

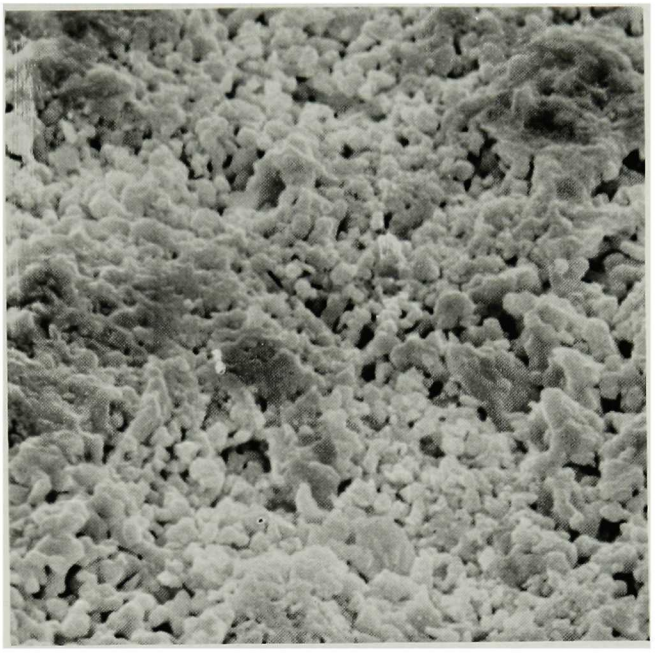

Fig. 3a. Porous Y_2O_3 Prepared from As-Received Powder (Magnification 300X)

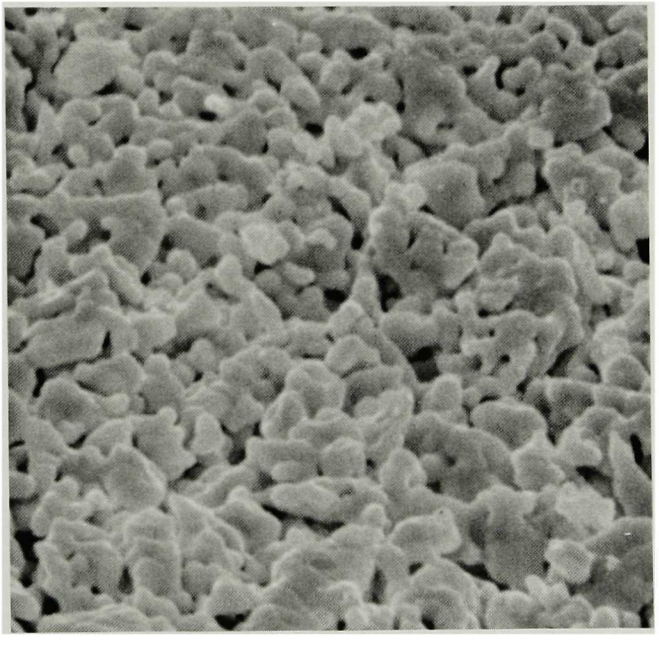

Fig. 3b. Porous Y_2O_3 Prepared from Calcined Y_2O_3 (Magnification 3000X)

Table IV-1. Permeabilities of Familiar Porous Substances

Material	Porosity	Permeability, millidarcies	References
SiO_2 Powder	0.37-0.49	13-51	5
Sand	0.37-0.50	20,000-18,000	5
Common Brick	0.12-0.34	4.8-220	5
Refractory Brick	0.15-0.22	70-1500	6
Coke	0.21	30-100	6
Limestone	0.04-0.10	0.2-45	5
Sandstone	0.08-0.38	0.5-3000	5
Specimen 3a	0.41	7.4	This report
Specimen 3b	0.36	11.4	This report

5. Material Studies

(J. A. Smaga and K. M. Myles)

The development of a reasonably low-cost alloy with suitable corrosion resistance in the positive electrode is one part of the present current-collector program. Initial investigations have focused on the corrosion behavior of iron-base alloys in the Fe-Mo-Ni ternary system (ANL-76-9, p. 46). One composition, Fe-30 wt % Ni-15 wt % Mo, was selected for additional evaluation and refinement.

AMAX Specialty Metals Corp. was contracted to fabricate a 0.25-mm (0.10-in.) sheet of the above alloy and was unable to roll this material without frequent heat treatments. This problem was not expected on the basis of preliminary rolling results.* Examination of samples from intermediate rolling steps revealed the presence of a "Chinese script" type phase, identified by the scanning electron microprobe† as rich in nickel and molybdenum. In the as-received 0.25-mm sheet, the second phase had been spheroidized and reduced in amount by the additional processing. This phase was evidently present throughout rolling owing to insufficient homogenization of the starting ingot.

To eliminate this second phase in the as-received material, portions of the alloy sheet were solution-annealed at 1225°C for time intervals ranging from 1 to 22 hr. Metallographic examination revealed that most of the second phase was eliminated after the shorter annealing times, and the material appeared homogeneous after the longer anneals. Static corrosion tests, conducted at 400°C for 500 and 1000 hr, confirmed these findings by showing declining corrosion rates with increasing annealing times. In an equal-volume mixture of FeS and LiCl-KCl, average corrosion rates of 67, 57, and 43 μm/yr were determined for the as-received alloy, the 1-hr solution-annealed condition, and the 22-hr solution-annealed condition, respectively. In a similar mixture of FeS_2 and LiCl-KCl,

*H. Thresh, ANL Materials Science Division.

†W. Shinn, ANL Chemical Engineering Division.

the rates were 1300, 1100, and 650 μm/yr for the same respective conditions. Furthermore, intergranular attack was minimized with the 22-hr anneal. The corrosion study in FeS_2 and LiCl-KCl indicates that further work is required to optimize the alloy composition for possible application in FeS_2 cells. The 0.25-mm alloy sheet in the annealed condition should be usable in FeS cells, and will be made available for such use. However, because excessive grain growth at 1225°C hinders fabrication, the current collector must be formed into the desired configuration prior to solution-annealing.

6. Cell Wetting Studies
(J. G. Eberhart)

A recurring problem in cell design is the wettability of the porous separator material by the molten-salt electrolyte. In an effort to improve penetration of the separator by the electrolyte, measurements were made of advancing and receding contact angles of various molten-salt electrolytes on hot-pressed BN surfaces. Over ordinary cell operating temperatures, LiCl-KCl eutectic from Lithcoa had the best wetting properties; LiCl-KCl eutectic from Anderson Physics Laboratory and a quaternary system of 2 wt % LiF-26% LiCl-11% KCl-61% $CaCl_2$ had intermediate wetting properties; and a salt composed of LiCl-KCl eutectic from Anderson Physics Laboratory and 13 wt % $CaCl_2$ had the poorest wetting properties. The advancing contact angles for all electrolytes showed nonwetting, whereas the receding angles all showed wetting, except for the LiCl-KCl-$CaCl_2$ salt. This poorest wetting salt was studied further by BN fabric penetration tests. Evacuation and abrupt repressurization of the test chamber only caused the salt to penetrate the larger spaces between the BN yarns, but not the smaller spaces between the fibers.*

Aluminum nitride (AlN) is being considered as an advanced cell separator material. Contact angle measurements showed that hot-pressed AlN has poorer wettability than BN for advancing salt, but better wettability for receding salt. Thus, AlN separators should be more difficult to penetrate with salt, but less subject to dewetting once it is penetrated.

Studies were also conducted on the tendency of the LiCl-KCl electrolyte to creep along metal surfaces. Creepage of electrolyte is believed to result from complete wetting of the steel cell housing and a gradient in the molten-salt surface tension (the Marangoni effect). Pure salt does not wet steel sufficiently well for creeping to occur. Thus, experiments were performed to observe the effect of Li-Al saturation on molten-salt wetting behavior. On a hot-pressed BN surface the addition of Li-Al powder to the salt made no significant difference in the wetting angles of the salt. On a Type 316 stainless steel surface, however, the pure salt, which was slightly nonwetting, spread over the surface within a minute after Li-Al was added to the salt. Thus, saturation with Li-Al appears to be the "cause" of electrolyte creepage. These experiments also suggest a simple remedy for the problem. A coating of a nonwettable ceramic (such as BN, AlN, or C) deposited on the upper inside surface of the cell housing (above the electrolyte level) would provide a barrier to the advancing electrolyte.

*In further tests, D. R. Vissers of the Cell Chemistry Group obtained some improvement in penetration through repeated evacuation and repressurization of the system.

7. Cell Degassing Studies
(J. G. Eberhart)

The degassing and the attendant pressure build-up which can occur during the operation of a cell is probably detrimental to its efficiency and lifetime. Thus, a study was initiated to characterize, by mass spectrometry, the gaseous species produced while cells are in a charge, discharge, or open-circuit mode. A vacuum system and a cell which permits visual observation of the electrodes have been designed for this study. Drawings have been submitted to the glass shop for fabrication of the vacuum system and cell.

8. Electrical Conductivity Studies
(J. G. Eberhart)

The electrical resistances of the various components of a cell have an important effect on its efficiency. Thus, a study was initiated on one of the key components of total cell resistance, namely, the electrical conductivity of molten LiCl-KCl electrolyte in which is dispersed a second, solid, nonconducting phase of cell separator material. The initial efforts of this study have involved an examination of the literature on the ionic conductivity of molten LiCl-KCl and the theories related to the conductivity of mixtures of conducting and nonconducting phases. Existing measurements and theories permit reliable estimation of the conductivity of some composite systems of interest to our program, and a separate report will be written on these two topics.

9. Postoperative Cell Examinations
(F. C. Mrazek, K. G. Carroll, J. E. Battles)

Postoperative examinations are conducted on test cells primarily to evaluate the performance of various construction materials and components--in particular feedthroughs, current collectors, electrode separators, and cell housings. These examinations provide important information, not only on the compatibility of cell components with other materials in the cell, but also on the performance and behavior of the Li-Al and metal-sulfide electrode materials. The examination procedures have been described previously (ANL-8109, p. 72).

Table IV-2 presents a summary of cells that were examined during this period, along with some conclusions as to the causes of cell failure. A major mode of cell failure was electrical short circuits caused by the extrusion of active material from one electrode and subsequent contact with the other electrode, as shown in Fig. IV-4. Another cause of short circuits was the presence of metallic and sulfide particles in the separator.

a. Lithium-Aluminum Analyses by Ion Microprobe Mass Analyzer (IMMA)

Major changes in handling procedures for metallographic samples have made possible the preparation of samples suitable for IMMA examination. This technique will permit determination of Li:Al ratios of the metallic particles at various locations in the negative electrodes of Li-Al/FeS_x cells.

Table IV-2. Summary of Cell Postoperative Examinations

Cell No.	Type of Cell	Days of Operation	Number of Cycles	Reason for Termination	Postoperative Examination
FM-2	Li-Al-Ca/ $FeS-Cu_2S$	77	127	Declining performance	This cell evaluated the effects of an 8 wt % Ca addition to the normal LiAl used in the negative electrode. Metallographic examination revealed a large amount of unusual crystalline material in the BN separator, later identified by X-ray diffraction and electron microprobe (EMP) as CaS. Further bulk analysis of the various portions of the cell showed that most of the Ca had migrated from the negative electrode into the separator.
R-24	$LiAl/FeS_2-CoS_2$	21	27	Short circuit	The short circuit in this cell was caused by massive upward extrusion of the positive electrode materials and its subsequent contact with the negative electrode.
A-3	$LiAl/FeS_2-CoS_2$	1	1	Short circuit	Very large aluminum particles plus small Al_2S_3 particles, as determined by EMP, were observed in the separator. The Al particles are believed to be responsible for the short circuit.
TO-3	$LiAl/FeS_2-CoS_2$	18	9	Short circuit	The negative electrode in this cell, originally a cast plaque of LiAl, more than doubled in thickness during cycling. This excessive expansion caused the short circuit by compressing the positive electrode and forcing positive electrode material through the bottom corner of the separator, and this material contacted the housing.

Table IV-2. Summary of Cell Postoperative Examination (Contd.)

Cell No.	Type of Cell	Days of Operation	Number of Cycles	Reason for Termination	Postoperative Examinations
EP-I-1-A-1	LiAl/FeS_2-CuS_2	30	34	Short circuit	Macroexamination showed that the short circuit was caused by inadequate restraint of the positive electrode which allowed it to move and contact the negative electrode frame.
R-15	LiAl/FeS_2-CoS_2	106	155	Short circuit	Microexamination revealed a large amount of metallic particles, in stringer-like formation, bridging the BN separator. These stringers are believed to be responsible for the massive short circuit condition throughout this cell. EMP showed these particles to be an Fe-Al alloy of varying composition.
R-25	LiAl/FeS_2-CoS_2	38	66	Short circuit	This cell's negative electrode was originally made by putting Li foil between layers of Al wire and electrochemically forming the LiAl. Microexamination showed that the Li foil had reacted and that the separator contained a metallic contaminant which, because of its highly reactive nature, may have been free Li. Further analyses are in progress to identify the material within the separator.
MP-2	LiAl/FeS_2-CoS_2	121	200	Short circuit	This cell was a multiplate design containing two carbon-bonded positive electrodes and four negative electrodes. A specific area of shorting could not be located but Fe and Al particles were observed in the separator.

Table IV-2. Summary of Cell Postoperative Examination (Contd.)

Cell No.	Type of Cell	Days of Operation	Number of Cycles	Reason for Termination	Postoperative Examinations
EP-I-2-2	LiAl/FeS-Cu_2S	15	20	Short circuit	This cell had a Y_2O_3 felt separator. The short circuit resulted from extrusion of positive electrode material through the corners of the felt because of inadequate retaining brackets within the electrode. The Y_2O_3 felt was free of active material in all other locations examined.
EP-1A8	LiAl/FeS-Cu_2S	62	164	Overcharged	Overcharging this cell by 0.3 V above the normal 1.6 V caused a rapid decline in performance. Catastrophic corrosion effects were observed on the mild steel current collector in the positive electrode. Large iron particles, ~150 μm long, encapsulated the separator fibers, thus indicating *in situ* formation.
TO-2	LiAl/FeS_2-CoS_2	11	7	Short circuit	The negative electrode was originally a cast plaque of solid LiAl. The back third of the plaque thickness was unreacted, whereas the remaining two-thirds was broken up into smaller particles. The large expansion of the negative electrode caused an upward extrusion of the positive electrode and a short circuit between the electrodes.

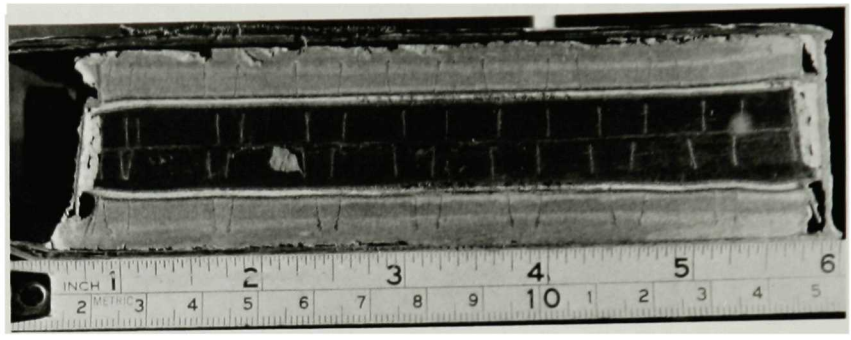

Fig. IV-4. Cross-section of Cell I-2-2 (extrusion of electrode material in lower left corner).

Application of this technique to the charged Li-Al electrode of Cell LT-2 indicated a substantial lithium concentration gradient across the thickness of the electrode. Lithium concentrations were as high as 68 at. % near the front face, as low as 6 at. % near the back face. a lithium concentration gradient had been previously indicated by earlier chemical analysis and microscopic examinations.

b. Formation of Li_2S in Electrode Separators

As previously described (ANL-77-17, p. 39) examinations of FeS_2 cells have shown the presence of a continuous band of Li_2S (with iron) in the electrode separators. This band is parallel to the electrode face, and generally located closer to the negative than to the positive electrode. Additional FeS_2 cells have been examined since ANL 77-17, and these cells along with the FeS_2 cell previously reported are listed in Table IV-3. Lithium sulfide was present in the separators of all FeS_2 cells in Table IV-3 with the exception of S-86, S-87, R-15, R-25 and A-3. The absence of Li_2S in the separators of cells S-86 and S-87, has been tentatively attributed to a reaction of FeS_2 with the Hastelloy B current collector which resulted in reduced sulfur activity, and to reduced charge cutoff voltage. The presence of Al_2S_3 and an Fe-Al intermetallic compound in the separator of Cell R-15 indicates that this cell was subjected to some abnormal conditions during operation. Cell A-3 also showed the presence of Al_2S_3 and large masses of aluminum metal which encapsulated the separator fibers; this behavior may have resulted from an overdischarge of the cell. The absence of Li_2S in the separator of this cell was attributed to the fact that a full charge to FeS_2 was not achieved.

The cells listed in Table IV-3 include those assembled in both the charged and uncharged states, and operated as upper-plateau and two-plateau cells. The data show no correlation between the presence of Li_2S and the type of cell (upper- or two-plateau) or assembly procedure. The only correlation observed thus far is that the cell must have a FeS_2 positive electrode, since Li_2S does not form in the separator of cells with FeS positive electrodes. This behavior suggests that the formation of Li_2S in the

Table IV-3. Separator Examinations of FeS_2 Cells

Cell No.	Li_2S in Separator	Temp., °C	Life, Days	Life, Cycles	Additive	Charge Cutoff Voltage, V
2B4	Yes	450[a]	79	140	Co-S	2.0
2A4	Yes	425-435[a]	114	409	Co-S	2.1
G-003	Yes	∿450	36	38	Co-S	overcharged
G-006	Yes	475	144	522	Co-S	2.0-2.1
EC-1	Yes	450[b]	5	25	Co-S	2.3
CCC-1	Yes	475	867	707	None	2.2-2.3
W-5	Yes	450	89	111	None	-----
W-9	Yes	450	62	76	None	-----
W-12	Yes	450	8	10	Co-S	-----
TO-3	Yes	430	18	9	Co-S	2.23→2.11
S-86[c]	No	450	219	405	Co-S	1.96 (1.80)[d]
S-87[c]	No	450	144	368	Co-S	1.96 (1.80)[d]
R-25[e]	No	450	38	66	Co-S	2.3
R-15	No	∿450[f]	107	155	Co-S	2.1
R-24	Yes	450	21	27	Co-S	2.1
TO-2	Yes	430	11	7	Co-S	2.1
A-3[g]	No	425	1	<1	Co-S	2.0
MP-2	Yes	450	121	200	Co-S	2.1
M-1	Yes	440	17	17	Co-S	2.12-2.20

[a] Peak power test conducted on these cells.

[b] Cell temperature 512°C during start-up.

[c] Hastelloy B current collector.

[d] Two different charge cutoff voltages used.

[e] Li metal or Li alloy observed in separator.

[f] Al_2S_3 and an intermetalic compound of Fe-Al observed in separator.

[g] Upper plateau, uncharged. Shorted before completion of first charge.

separator is related to the high sulfur activity in FeS_2 cells and may be prevented by reducing the sulfur activity. This effect was observed in cells S-86 and S-87.

B. Cell Chemistry
(M. F. Roche)

The objectives of the cell chemistry studies are (1) to investigate specific chemical and electrochemical problems that arise in the development of cells and batteries, (2) to conduct studies that are expected to lead to improvements in the electrodes and in cell design, and (3) to provide a basic understanding of the processes that occur within cells.

1. Studies of Sulfur and Iron Losses from FeS_2 Electrodes (A. E. Martin, Z. Tomczuk, M. F. Roche)

Powders of FeS_2, $FeS_2 + Li_2FeS_2$, or $FeS_2 + Li_2S$ were added to LiCl-KCl electrolyte and these mixtures were heated at 700 K in 6 cm^3 alumina crucibles that were open to a helium glove-box atmosphere. The mixtures consisted of about 0.2 g of each powder in 1 g of electrolyte. Assuming that the weight losses were from the FeS_2 fraction in each mixture, the FeS_2 lost 2.4% of its original weight in 3 days and 2.5% in 6 days. For the $Fe_2S + Li_2FeS_2$ mixture, no significant weight loss was detected. However, substantial losses, namely 4.9% in 3 days and 8.3% in 6 days, were obtained with the $Li_2S + FeS_2$ mixture. Thus, the Li_2S appeared to accelerate the weight loss of the FeS_2. Because the vapor pressure of sulfur over FeS_2 is only 7.3×10^{-2} Pa (7.2×10^{-7} atm) at 700 K[8], the high initial loss (first 3 days) for the mixture of FeS_2 in electrolyte is surprising. The expected change in sulfur/iron ratio for this sample was not confirmed metallograpically.

Metallographic examinations were conducted on the products of the three tests. Because of the observed weight loss in the FeS_2-electrolyte mixture, a superficial layer of $Fe_{1-x}S$ was expected to have formed on the FeS_2 particles, but no layer of any kind was detected. The mixture of FeS_2 and Li_2FeS_2 had been converted to FeS_2, $Li_4Fe_2S_5$, and Fe_{1-x}, with loose layers of $Li_4Fe_2S_5$ on the FeS_2 particles. In the Li_2S and FeS_2 mixture, a reaction layer had formed on the FeS_2 particles. This reaction layer was recognized as a phase previously observed when Li_2S and FeS_2 powders were reacted in the absence of electrolyte. In these earlier tests, the composition of this phase was estimated to be $Li_6Fe_3S_8$, which is slightly more sulfur-rich than $Li_4Fe_2S_5$.

Thermodynamic calculations based on emf measurements of cells (ANL-77-17, p. 46) and literature data[8] indicate that the reaction $2FeS_2 + 2Li_2S \rightarrow Li_4Fe_2S_5 + S$ exerts a sulfur vapor pressure of 26 kPa (0.25 atm) at 700 K (sulfur activity of 0.335). Thus, the thermodynamic calculations lend support to the observation of a high sulfur loss for mixtures of Li_2S and FeS_2.

Evidence for formation of a yellow-orange solution species upon heating mixtures of Li_2S, FeS_2 and LiCl-KCl electrolyte has been reported.[9] Preliminary measurements of the iron and sulfur concentration of this solution were made. Lithium sulfide (2 g) and FeS_2 (2 g) were held in an alumina cylinder having a press-fit porous graphite face. This assembly was placed in 255 g of LiCl-KCl electrolyte, and was equilibrated for 24 hr at three temperatures (718, 736, and 776 K). During this equilibration, the electrolyte was stirred to promote transport of soluble species through the porous graphite into the electrolyte bath. Samples of the electrolyte were then taken in U-shaped quartz sampling tubes. The frozen samples had a yellowish orange color. The results of analyses* for iron and sulfur are compared with earlier results for Li_2S alone and FeS_2 alone in Table IV-4.[10]

*Analyses performed by K. J. Jensen, Analytical Chemistry Laboratory.

Table IV-4. Analyses of LiCl-KCl Electrolyte Equilibrated with Li_2S, FeS_2, or Li_2S and FeS_2 (ppm[a])

			Li_2S and FeS_2[b]	
T,K	Li_2S	FeS_2	Li_2S	FeS_2
718	1080	35	90	38
737	1300	42	600	37
776	1870	59	2400	47

[a] Micrograms of compound per gram of LiCl-KCl electrolyte.

[b] Iron was assumed to be present as FeS_2; the remainder of the sulfur was assumed to be Li_2S.

Although all the solutions were highly colored, only small amounts of iron were found. These preliminary results suggest that the species responsible for the solution color is not present at an unusually high concentration. However, in view of the sulfur vapor losses over Li_2S-FeS_2 mixtures, some method of sealing the system to prevent vapor losses must be devised to obtain accurate solubility data.

The situation described in the above experiments (coexistence of Li_2S and FeS_2) is not one that is normally encountered during cell operation; FeS_2 is present near full charge, whereas Li_2S is formed later in the discharge. However, the tests suggest that Li_2S in the BN separator of a cell will not be readily absorbed by a positive electrode that is rich in FeS_2.

A variety of other possible abnormal situations that might exist during charging of the positive electrode have been subjected to a preliminary thermodynamic analysis, but have not been observed experimentally. Calculated emfs (ANL-77-17, p. 47) for some reactions that are capable of producing the undesirable species, $FeCl_2$ or liquid sulfur, are:

$$Li_2S + 2Al \rightarrow S + 2LiAl \qquad 1.87\ V$$

$$Li_4Fe_2S_5 + 4Al \rightarrow S + 4LiAl + 2FeS_2 \qquad 1.85\ V$$

$$2FeS + 2Al + 2LiCl \rightarrow FeCl_2(10^{-3}M) + 2LiAl + FeS_2 \qquad 1.97\ V$$

$$FeS_2 + 2Al + 2LiCl \rightarrow FeCl_2(10^{-3}M) + 2S + 2LiAl \qquad 2.33\ V$$

The first three reactions might occur in positive-electrode regions rich in Li_2S, $Li_4Fe_2S_5$, or FeS; the emfs of these reactions are lower than the charge-cutoff voltage of 2.2 V normally used in $LiAl/FeS_2$ cells. The last reaction is prevented by use of a 2.2 V charge cutoff. Additives capable of preventing formation and escape of sulfur or $FeCl_2$ are now being sought.

2. Titanium Disulfide Electrode Development
(K. E. Anderson, D. R. Vissers)

Tests of a 1 A-hr (0.2 A-hr/cm^2) TiS_2 cell indicated that this electrode operates well (ANL-77-17, p. 47). The electrode contained only 15% electrolyte by volume after cycling; however, this low volume fraction of electrolyte did not limit the TiS_2 utilization. A utilization of 97% was obtained at a discharge current density of 100 mA/cm^2.

Larger scale tests of TiS_2 are now being conducted. A prismatic cell (12.5 x 12.5 x 4.4 cm) was constructed with a 2-cm-thick, 142 A-hr TiS_2 positive electrode sandwiched between two 0.7-cm-thick, 75 A-hr LiAl negative electrodes. The TiS_2 was cold-pressed without electrolyte onto a molybdenum current collector at 75 tons (6.8 x 10^4 kg) to a density of 2.05 g/cm^3 (64% of theoretical). The cell was operated at 430°C. Its resistance was 6 mΩ and its average discharge voltage was 1.7 V. The achieved capacity at 10-A discharge and charge currents (33 mA/cm^2) was 90 A-hr, which corresponds to a specific energy of 54 W-hr/kg.

At 20-A discharge and charge currents the capacity was 70 A-hr. During the seventh charge, the charge-cutoff voltage was increased from 2.28 to 2.33 V in an attempt to increase the specific energy. This higher cutoff voltage caused the coulombic efficiency to decline from 95% to about 30% by cycle 17, at which time the test was terminated. The cell was then cross-sectioned and examined. The positive electrode had expanded by 30%, to a thickness of 2.6 cm. The BN fabric separator, located between the LiAl and TiS_2 electrodes, had become conductive. This effect probably occurred because liquid lithium, which formed in the negative electrodes as a result of the high charging voltage, had penetrated through the separator.

In spite of the problems with the first engineering-scale TiS_2 cell, the system appears to be promising. Additional cells are now being fabricated to better characterize the TiS_2 electrode.

3. Performance of Li-Al Electrodes with Additives
(D. R. Vissers and K. E. Anderson)

Investigations are continuing on modifications of the Li-Al electrode that may result in sustained high capacities during extended cycling. It is suspected that the decreasing capacity of the Li-Al electrodes results from morphological changes of the active material over a period of time. The present studies are focused on the use of various metallic additives to the Li-Al binary alloy as a possible means of controlling or modifying these morphological changes. The additives that are currently under investigation are indium, lead, tin, and copper.

The Li-Al-M (M = metal additive) electrodes were prepared by melting mixtures of the desired composition at about 800-900°C in tantalum crucibles.* The alloy was ground to a powder and placed in an iron Retimet

*These materials were prepared by A. E. Martin.

disk, which was enclosed in a 325-mesh stainless steel screen basket to contain the particulate material. This electrode was operated against a liquid-lithium counter electrode with the same area (15.6 cm^2) in LiCl-KCl electrolyte at ∿425°C. The Li-Al-M electrodes were about 0.8 cm thick, and had theoretical capacities of approximately 10 A-hr.

The performance of the ternary-alloy electrodes was evaluated by comparing the capacity of the cells at various current densities (0.05 to 0.10 A/cm^2 during charge and 0.05 to 0.30 A/cm^2 during discharge). The IR-free cutoff potentials for discharge and charge were 0.15 and 0.70 V, respectively; these cutoffs permitted a polarization of the LiAl electrode that is similar to its polarization in LiAl/metal sulfide cells. Early results were reported in ANL-76-98, p. 44.

The latest results of this study of additives are summarized in Table IV-5. Additions of lead (10 wt %), tin (5 wt%), or copper (5 wt %) did not improve the capacity retention characteristics of the electrodes, although the tin addition improved the capacity density during early cycling. In contrast, the addition of indium (3.9 wt %) greatly improved the capacity retention; the rate of capacity decline per cycle was <0.01%, as compared with a rate of 0.06% for a Li-Al electrode with no additive. Photomicrographic examination of the test electrodes showed that the major morphological differences exhibited by the Li-Al-In electrode was the presence of dendritic particles with high surface area. Studies are being continued with additivies of antimony and zinc.

C. Advanced Battery Research
(M. F. Roche)

The objective of this work is to develop new secondary cells that use inexpensive, abundant materials. The experimental work ranges from cyclic voltametry studies and preliminary cell tests through the construction and operation of engineering-scale cells for the most promising systems. The studies at present are focused on the development of new cells with molten-salt electrolytes.

1. Cyclic Voltammetry Studies
(S. K. Preto, M. F. Roche)

Cyclic voltammetry is being used to investigate the electrochemical behavior of candidate electrode materials for cells that have calcium negative electrodes and molten-salt electrolytes. Results for Ca-Al electrodes in NaCl-$CaCl_2$ electrolyte and LiAl electrodes in LiCl-KCl electrolyte were presented in a previous report (ANL-76-81, p. 49). Results for electrodes with intermetallic compounds (calcium and aluminum, magnesium, or Mg_2Si) in LiCl-KCl-$CaCl_2$ electrolyte as well as results for FeS electrodes in either LiCl-KCl or LiCl-KCl-$CaCl_2$ electrolyte are presented in this report. In LiCl-KCl, the reference and counter electrodes were LiAl + aluminum; in LiCl-KCl-$CaCl_2$, they were $CaAl_4$ plus aluminum. The working electrodes for the calcium intermetallics were contained in iron housings of 3-cm^2 area and 0.4-cm thickness. Iron sulfide working electrodes were loaded into molybdenum housings of 5-cm^2 area and 0.3-cm thickness.

Table IV-5. Performance and Capacity Retention of LiAl Electrodes with Additives

Additive	Charge Current Density mA/cm^2	Utilization[a] at Discharge Current Density				Capacity Decline,[b] %/cycle	Utilization[b]
		50 mA/cm^2	100 mA/cm^2	200 mA/cm^2	300 mA/cm^2		
None	50	92.3	89.2	84.6	81.9	0.06	87.0
	100	80.2	76.6	76.6	65.6		
3.9 wt % In	50	92.7	90.5	88.6	83.2	<0.01	89.2
	100	70.0	70.0	70.0	65.4		
1 wt % In	50	92.2	90.4	83.8	71.7	<0.01	90.3
	100	90.4	80.1	82.7	74.1		
5 wt % Sn	50	94.1	92.4	90.6	83.7	0.14	82.8
	100	81.9	81.9	81.9	78.4		
10 wt % Pb	50	92.2	90.2	86.2	84.2	0.30	77.0
	100	82.2	74.1	74.1	72.1		
5 wt % Cu	50	98.6	96.6	83.7	80.9	0.06	83.0
	100	66.7	65.9	65.3	63.5		

[a]Percent of theoretical lithium capacity. Data obtained during first 50 cycles.

[b]Measured at 50 mA/cm^2 charge and discharge current densities after 100 cycles.

The Ca-Al voltammetry results were essentially the same in LiCl-14.5 mol % KCl-31 mol % $CaCl_2$ at 500°C and in LiCl-37 mol % KCl-9 mol % $CaCl_2$ at 485°C. A voltammogram from the study in the former electrolyte is shown in Fig. IV-5. In addition to the Ca-Al doublet, which is also found in the NaCl-$CaCl_2$ electrolyte (ANL-76-81, p. 49), a LiAl peak is clearly evident on the cathodic side. It is present because of incomplete utilization of the aluminum by calcium reactions, which leaves some aluminum available for LiAl formation. The peak is absent on discharge because the LiAl reacts with $CaCl_2$ in the electrolyte to form LiCl and the calcium-aluminum compounds. As the working electrode was cycled, the LiAl peak became smaller relative to the calcium peaks, thereby indicating that breakup of the initially coarse aluminum particles permitted the calcium reactions to proceed more readily. A Ca-Mg voltammogram in LiCl-37 mol % KCl-9 mol % $CaCl_2$ at 457°C is shown in Fig. IV-6. Here the lithium interaction was not observed; lithium does not form a Li-Mg compound. A voltammogram for the ternary Ca-Mg-Si electrode is shown in Fig. IV-7. Its complexity precludes peak assignments.

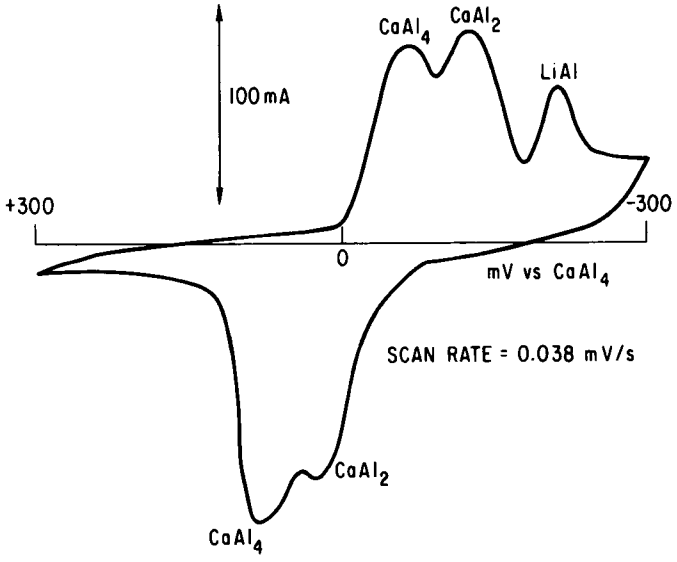

Fig. IV-5. Voltammogram for 200 mg Aluminum in LiCl-KCl-$CaCl_2$ at 500°C.

After 10 to 20 cycles to permit electrode formation, the percent utilization of the elctrode at various scan rates was determined by measuring the areas of the discharge peaks (in mA-hr) and comparing these values with the theoretical electrode capacities. The results for $CaAl_2$, $CaMg_2$, and $Ca_x(Mg_2Si)$ in LiCl-37 mol % KCl-9 mol % $CaCl_2$ at 485, 457, and 450°C, respectively, and for LiAl in LiCl-KCl (eutectic) at 465°C are given in Fig. IV-8. These electrodes had 50-70 mA-hr/cm^2 theoretical capacity densities. A scan rate of 0.1 mV/s is roughly equivalent to a 1-hr charge and discharge of the electrodes. The very good performance of LiAl is attributed to the very high permeability of lithium through aluminum and the intermetallic[11] compound LiAl. The solubility of lithium in aluminum and in LiAl is about 10 at. %, but

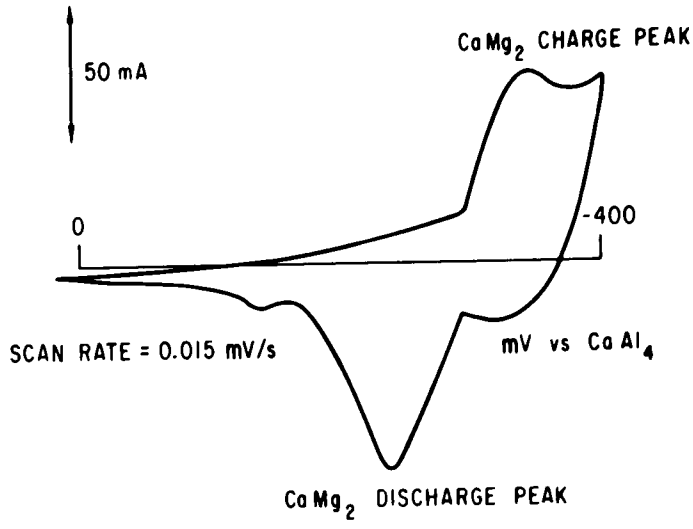

Fig. IV-6. Voltammogram for 364 mg $CaMg_2$ in LiCl-KCl-$CaCl_2$ at 457°C

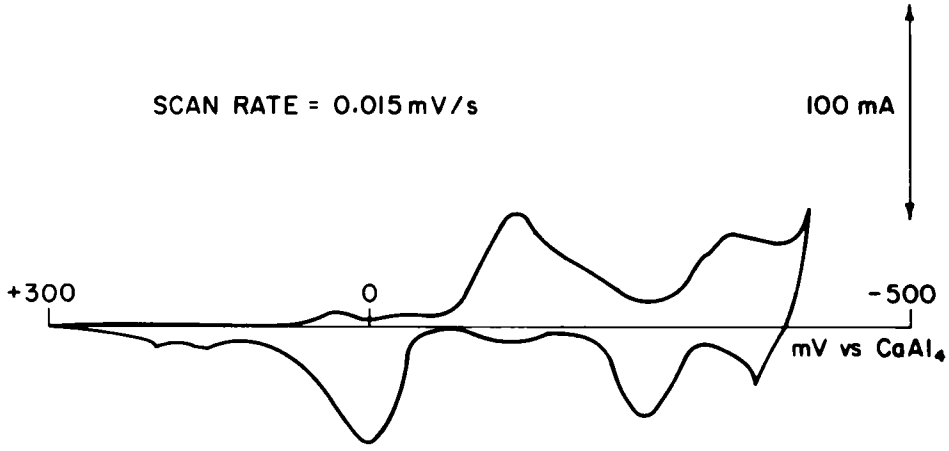

Fig. IV-7. Voltammogram for 200 mg Mg_2Si in LiCl-KCl-$CaCl_2$ at 460°C

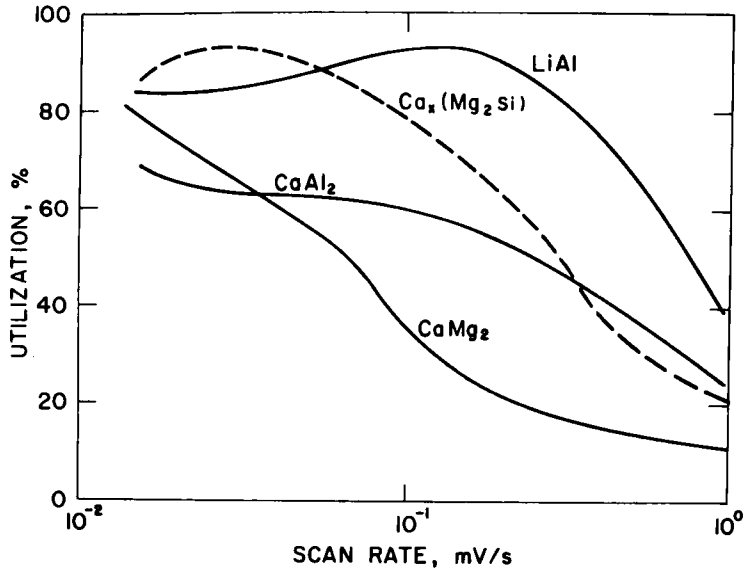

Fig. IV-8. Percent Utilization *vs.* Voltammetric Scan Rate for LiAl, $CaAl_2$, $CaMg_2$, and $Ca_x(Mg_2Si)$

the solubility of calcium in the phases that exist in binary calcium systems is generally less than 1 at. %.[12] This lower solubility (and probably a lower diffusion coefficient for calcium than for lithium) restricts the performance of the binary calcium intermetallic electrodes. However, in-cell tests have demonstrated that the Ca-Mg-Si ternary system performs better than $CaAl_2$ or $CaMg_2$ and approaches the performance of LiAl (ANL-77-17, p. 53). Voltammetry results in Fig. IV-8 for a 70 mg/cm^2 Mg_2Si electrode support this finding: assuming 1 A-hr Ca/g Mg_2Si theoretical capacity, the utilization in LiCl-37 mol % KCl-9 mol % $CaCl_2$ at 460°C was 90% at a scan rate of 0.025 mV/s, 77% at 0.10 mV/s, and 24% at 1 mV/s.

The behavior of FeS in LiCl-KCl eutectic is illustrated in Fig. IV-9. The voltammogram shown is typical; the current traces overlay one another on repeated cycling. The peaks below the axis (discharge) are interpretable because of a metallographic study (ANL-77-17, p. 42) which showed that the surface and interior of FeS particles had different discharge paths. Briefly, the three discharge peaks, reading from right to left are assigned to: (1) discharge of the particle surface to J phase ($LiK_6Fe_{24}S_{26}Cl$), (2) discharge of the interior of the particles (via Li_2FeS_2) to Li_2S and Fe, and (3) discharge of the J phase on the surface to Li_2S and Fe. The dominant discharge peak is quite broad; it is believed to be a doublet that is unresolved because the discharge is occurring through a J-phase layer. The peaks above the axis (charge) suggest a charge mechanism that is quite simple compared with the discharge mechanism. Each peak represents 50% of the charge. The first peak represents the formation of Li_2FeS_2 from Fe and Li_2S, and the second peak represents the further reaction of Fe and Li_2FeS_2 to form FeS. J-phase formation may occur as an intermediate step during the second charge peak, and is frequently observed metallographically in charged FeS cells. This study of the reactions of lithium ions with FeS was made to aid in understanding the behavior of FeS in the presence of calcium ions.

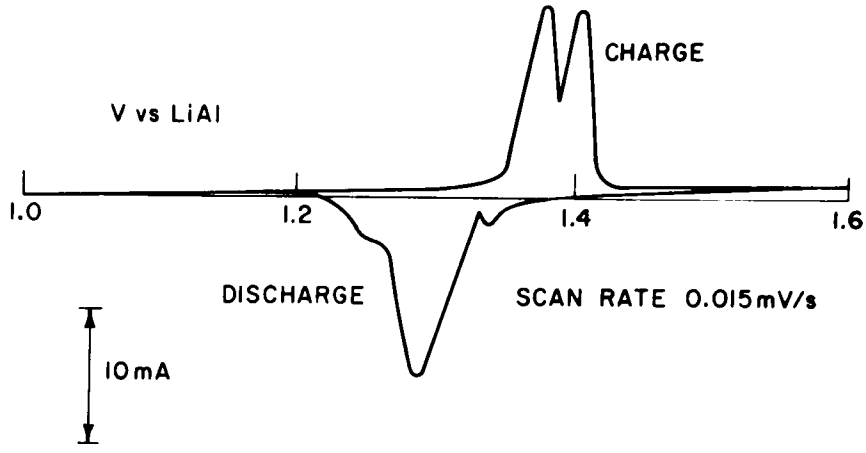

Fig. IV-9. Voltammogram for 20 mA-hr FeS and 100 mg Fe Powder in LiCl-KCl at 430°C

The behavior of FeS in LiCl-37 mol % KCl-9 mol % $CaCl_2$ is illustrated in Fig. IV-10. The major charge and discharge peaks result from the calcium-ion reaction. The minor (unlabeled) peaks, which are at a lower voltage than the calcium-ion peaks, result from the lithium-ion reactions just described. These lithium-ion peaks are initially larger than the calcium-ion peak, but become smaller with cycling and eventually disappear as the electrode particles become very fine.

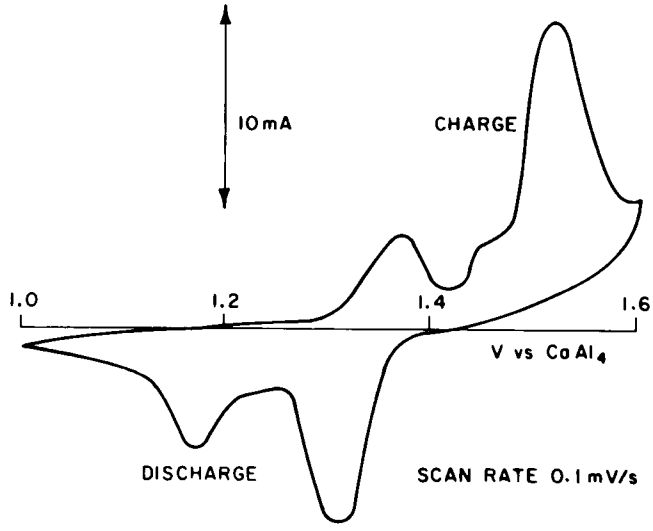

Fig. IV-10. Voltammogram for 20 mA-hr FeS and 100 mg Fe Powder in LiCl-KCl-$CaCl_2$ at 460°C

A major problem, particularly noticeable in this voltammogram, is that the FeS charge peak (above the axis) is located on a general upsweep in current that results from a highly undesirable side reaction--the formation of soluble $FeCl_2$ by oxidation of iron. The upsweep (between 1.4 and 1.6 V) is so pronounced because only 10% utilization of the FeS was achieved in this test. The problem of iron oxidation was largely eliminated in a later experiment in which no excess iron was added and the FeS was incorporated into a carbon-foam current collector. The FeS utilization in this later experiment was 60%, which was the same as the utilization in the lithium-ion voltammetry experiment of Fig. IV-9. These experiments indicate that distributed carbon, not iron, is a satisfactory current collector for the FeS electrode in a calcium system.

2. Utilization of Iron Sulfides
(Z. Tomczuk, A. E. Martin)

Positive electrodes of FeS or FeS_2 having capacities of 1 to 2 A-hr were prepared in small, graphite housings of 5-cm^2 area and 0.6-cm thickness. The utilization of the theoretical capacity at a current density of 10 mA/cm^2 was measured at 450°C in LiCl-KCl eutectic, LiCl-37 mol % KCl-9 mol % $CaCl_2$, or NaCl-20 mol % KCl-50 mol % $MgCl_2$. The negative electrodes consisted of Li, $CaAl_2$, and Mg, respectively, and had much larger capacities than the positive electrodes. The results, which are summarized in Table IV-6, indicate that iron-sulfide electrodes in calcium and magnesium cells require added current collector (*e.g.*, carbon powder distributed throughout the active material) to obtain adequate utilization. (Iron provides adequate current collection, but is too easily oxidized to be practical.) Optimization of the current-collector material and design may lead to utilizations greater than 90%.

Metallographic studies revealed that, in the absense of added current collector, layers of CaS or MgS, which are probably nonconductive, were formed on the iron sulfides only in the region near the graphite housing. These layers appear to have prevented electronic conduction to the iron sulfide particles that were not in direct contact with the housing.

In the lithium systems a separate Li_2S phase does not form with either FeS or FeS_2 until 50% utilization is achieved. This Li_2S is probably still a good electronic conductor since it contains a substantial amount of dissolved FeS (about 10 at. %). The iron sulfides themselves are known to be fairly good electronic conductors; the very high utilization (>90%) in the lithium-ion systems indicates that other sulfides, formed as the electrode discharges (*e.g.*, $Li_4Fe_2S_5$ and Li_2FeS_2), are also good electronic conductors.

3. Engineering Studies
(J. D. Arntzen, K. E. Anderson, D. R. Vissers)

Engineering-scale tests of the calcium/iron sulfide system have concentrated on evaluations of various negative electrodes ($CaAl_2$, Ca_2Si, $CaMg_2$, and Ca_xMg_2Si) in conjuction with an FeS positive electrode (ANL-77-17, p. 54). The FeS positive electrodes have had iron current collectors that oxidize to form $FeCl_2$ in solution while FeS is being generated from iron

Table IV-6. Utilization of Iron Sulfide Electrodes

	% Utilization
With Lithium Ions	
FeS	>90
FeS_2	>90
With Calcium Ions	
FeS	10
FeS_2	5
[a]FeS + Fe Retimet	70
FeS_2 + carbon	70
FeS_2 (15 wt % CoS_2) + carbon	70
With Magnesium Ions	
FeS_2	50
FeS_2 + carbon	70

[a]This test was conducted with the materials in an iron housing.

and CaS (see Sect. IV. C. 1). (This problem is not serious in lithium/iron sulfide cells because FeS forms from Fe and Li_2S at a lower potential.) The $FeCl_2$ forms an iron deposit on the negative electrode and, if this deposit penetrates through the separator, a short circuit should occur. This would explain many of the short circuits in the recent engineering-scale calcium cells. The laboratory-scale calcium cells have generally had high coulombic efficiencies. These cells were operated with an electrode separation of about 0.5 cm which eliminated the possibility of shorting by a separator that had become conductive. On the other hand, engineering-scale cells were operated with the electrodes pressed against 2-mm-thick BN cloth, and this condition increased the probability of short circuits. Current-collector oxidation can also cause poor electrode utilization if gaps between the current collector and active material are formed as a result of the oxidation process.

The seriousness of the iron oxidation problem in the calcium cells has been only recently recognized. The cells tested during this reporting period had iron current collectors. Two uncharged, prismatic (12.5 x 12.5 x 4 cm) calcium cells, CA-10 and -11, were fabricated and tested. The positive electrode of each cell consisted of hot-pressed mixture of CaS, Fe, and LiCl-37 mol% KCl-8 mol % $CaCl_2$ powders. In Cell CA-10 half of the mixture was pressed onto each side of an iron current-collector sheet. In Cell CA-11, six sheets of expanded iron mesh and 5 wt % acetylene black were incorporated into the hot-pressed mixture. The two uncharged, negative electrodes of each cell (one on each side of the positive electrode) contained a total of about 130 g Mg_2Si (approximately 130 A-hr) in iron Retimet current collectors.

The resistance of the cells was 6-7 mΩ, which is about the same as that of lithium-aluminum/iron sulfide cells. Cell CA-10 operated with about 90% coulombic efficiency through 46 cycles. The efficiency declined to about 75% by cycle 80, and the test was terminated after the coulombic efficiency had dropped to 65% (cycle 105). The best achieved capacity was 53 A-hr with a 10-A discharge current preceded by a trickle charge. Cell CA-11 had an achieved capacity of 40 A-hr (8-hr charges and discharges). It operated with about 90% coulombic efficiency for 27 cycles, but the efficiency declined to 66% by cycle 42. This cell had much more iron in the positive electrode than Cell CA-10, and exhibited a voltage plateau at 1.83 V during 10-A charges that might have resulted from iron oxidation. Both cells will be examined metallographically to determine the source of the short circuits. Future cells will incorporate other current collectors, such as carbon, nickel, and Hastelloy B, to avoid the current-collector oxidation problem.

V. LiS/FeS BATTERY PROGRAM--ATOMICS INTERNATIONAL

Emphasis has been placed on the construction of compact, uncharged bicells using powdered AlN separators during this period. Substitution of this powdered ceramic material for the rigid, porous Si_3N_4 plates or the plasma-sprayed BN cloth used earlier may provide increased cycle life in these cells, and has resulted in higher capacity utilization of the FeS active positive material. Increased cell life is anticipated in view of the excellent thermodynamic stability of AlN toward lithium. Higher capacity utilization, now approaching 80%, is believed to result from the low density (50%) of the powder separator with lower consequent lithium ion diffusion gradients. One cell of this type has completed 113 cycles and 100 days with 99% coulombic efficiency throughout its life.

Preparations are being made to characterize AlN and Y_2O_3 powders with respect to particle size and impurity levels. The effects of these variables on separator performance will be measured by in-cell tests. Work on the preparation of highly porous rigid AlN separators will be continued.

Operation of a 1.0 kW-hr Li_4Si/FeS-20 mol % Cu_2S cell was terminated after 330 cycles and 142 days of operation. The coulombic efficiency of this cell, which was above 95% during the first 150 cycles, declined to about 65% at the point of test termination. Subsequent sectioning and examination of this cell at ANL disclosed that the probable causes of cell failure were migration of copper from the positive electrode and corrosion of the BN cloth separator which had been plasma-sprayed with $MgO \cdot Al_2O_3$ spinel.

A 1.0 kW-hr cell equipped with a large number of thermocouples located at selected points within the cell is being placed in operation. Data will be collected at various charge and discharge rates to provide an experimental basis for determining thermal gradients in large load-leveling cells. A cell model is being prepared, and correlation of the model with experimental results is planned.

Design of a 2.5 kW-hr pre-prototype load-leveling cell has been initiated. This cell design will be based upon uncharged cell assembly technology and powder separators, assuming that full-scale bicells employing powder separators, currently being fabricated, are tested successfully.

REFERENCES

1. W. Towle, et al., *Cost Estimate for the Commercial Manufacture of Lithium/Iron Sulfide Cells for Load Leveling*, ANL-76-12 (March 1976).

2. W. F. Hamilton, *Impact of Future Use of Electric Cars in the Los Angeles Region: Volume I*, EPA-460/3-74-020-a, p. 10, October 1974.

3. J. J. Lander, *Requirements and Characteristics of Secondary Battery Separators*, Proc. of the Electrochem. Soc. Symp. on Battery Separators, Columbus, Ohio, p. 5 (1970).

4. G. D. Joglekar and V. K. Batra, *Pore Structure and Performance of Battery Separators*, J. of Scientific and Industrial Research, 19B, 312 (1960).

5. R. E. Collins, *Flow of Fluids Through Porous Materials*, Reinhold, New York, p. 10 (1961).

6. G. R. Eusner and J. T. Shapland, *Permeability of Blast-Furnace Refractories*, J. Amer. Ceram. Soc. 42 (10), 459 (1959).

7. American Society for Testing and Materials, *Annual Book ASTM Standards: Permeability of Refractories*, Part 17, p. 529 (1975).

8. K. C. Mills, *Thermodynamic Data for Inorganic Sulphides, Selenides and Tellurides*, Butterworths and Co., Ltd., London (1974).

9. Z. Tomczuk, et al., *Overcharge Studies of the FeS_2 Electrode in Li/FeS_2 Cells*, Proc. Symp. and Workshop on Adv. Battery Research and Design, ANL-76-8 (1976).

10. J. E. Hall, participant in undergraduate research program at *Argonne National Laboratory*, unpublished data, 1976.

11. M. Hansen and K. Anderko, *Constitution of Binary Alloys*, McGraw-Hill, New York, p. 104 (1969).

12. Ibid., p. 76.

APPENDIX A.

SUMMARY OF LARGE-SCALE CELL TESTS

APPENDIX A. Summary of Large-Scale Cell Tests

Cell or Battery No.	Type of Cell	Operating Characteristics: Capacity, A-hr: Theor.	Operating Characteristics: Capacity, A-hr: Max.[a] at Indicated Rates	Operating Characteristics: Rates, hr: Disch.	Operating Characteristics: Rates, hr: Charge	Initial Eff.,[b] %: A-hr	Initial Eff.,[b] %: W-hr	Life Characteristics: Days[c]	Life Characteristics: Cycles[c]	Life Characteristics: % Decline in: Capacity[d]	Life Characteristics: % Decline in: A-hr Eff.	Remarks
2A5	Li-Al/ FeS_2-CoS_2	69	55.6	5.6	5.6	99+	83	127	310	310	8.7	Eagle-Picher thin electrodes, Type A baseline cell. Max. specific energy, 65.8 W-hr/kg (5.6 hr rate); 41.6 W-hr/kg (4.1 hr rate) at 200 cycles. Terminated.
2B6	Li-Al/ FeS_2-CoS_2	149	117 68	11.6 4.5	11.6 4.5	99+	>84	>161	>221	27	16	Eagle-Picher thick electrodes, used in evaluation of cell heating and cooling. Cycled without equalization charge.
2B7	Li-Al/ FeS_2-CoS_2	149	124 91	9.5 4.0	9.5 7.0	99+	78	106	525	39	6	Eagle-Picher thick electrode baseline cell. Operated on 7 day electric vehicle cycling schedule. Terminated.
2B8	Li-Al/ FeS_2-CoS_2	149	118	11.8	11.8	99	>82	>223	>354	37	17	Start-up and operation with cell blanketed in Kaowool insulation, exposed to air.
02-002	Li-Al/ FeS-Cu_2S	168	133 103	13 4.1	13 10	99	86	52	43	0	1	Gould baseline design: 12.7 x 17.8 cm FeS cell (Ca additive in negative electrode). Specific energy, 44 W-hr/kg at 4-hr rate. Cell on standby.
03-002	Li-Al/ FeS-Cu_2S	168	111	5.1	11	99	80	64	79	3	0	Gould baseline design: 12.7 x 17.8 cm FeS cell (no Ca additive in negative electrode). Specific energy, 44 W-hr/kg at 4-hr rate. Cell on standby.
I-1-B-1	Li-Al/ FeS-Cu_2S	148	108 52	10.8 2.1	10.8 5.2	99	80	65	66	0	0	Test of Y_2O_3 separator in Eagle-Picher FeS, redesigned cell. Terminated, shorting.
I-2-2	Li-Al/ FeS-Cu_2S	148	90	9	9	-	-	15	20	-	-	Duplicate I-2-1. Retested. Terminated, declining coulombic efficiency. Y_2O_3 test.
I-3-A-1	Li-Al/ FeS-Cu_2S	150	125	12	12	99+	81.5	24	20	20	1	Baseline 1B Type Eagle-Picher cell test of NaCl additive to LiCL-KCl. Cell on standby.
I-3-A-2	Li-Al/ FeS-Cu_2S	148	103	10	10	99	84	27	31	0	0	Baseline 1B Type Eagle-Picher cell, 0.64 cm terminal rod. Cell on standby.
I-4-B-1	Li-Al/ FeS-Cu_2S	127	101 98 76	10 5.9 3.4	10 5.9 3.4	99+	81	>53	>73	1.5	0	Thinner positive, greater negative/positive ratio than Type B. 67 W-hr/kg at 10-hr rate.

[a] Based on at least five cycles.

[b] Based on at least 10 cycles at the 5-hr rate.

[c] The "greater than" symbols denote continuing operation.

[d] Percent decline from maximum capacity at the 5-hr rate, except where noted.

Cell or Battery No.	Type of Cell	Operating Characteristics: Capacity, A-hr: Theor.	Operating Characteristics: Capacity, A-hr: Max.[a] at Indicated Rates	Operating Characteristics: Rates, hr: Disch.	Operating Characteristics: Rates, hr: Charge	Initial Eff.,[b] %: A-hr	Initial Eff.,[b] %: W-hr	Life Characteristics: Days[c]	Life Characteristics: Cycles[c]	Life Characteristics: % Decline in: Capacity[d]	Life Characteristics: % Decline in: A-hr Eff.	Remarks
I-3-B-2	Li-Al/ $FeS-Cu_2S$	127	107	10.7	10	99+	82	>16	>15	0	0	Thinner positive, greater negative/ positive ratio than Type B, 67 W-hr/kg at 10-hr rate.
PC-1-01	Li-Al/ $FeS-Cu_2S$	136	90 64	9 2.5	9 6.4	99	86	>102	>137	0	0	Test of pellet-cell concept for making large electrodes. Specific energy 37 W-hr/ kg at 2.5-hr rate. Peak specific power, 45 W/kg.
R-23	Li-Al/ FeS_2+CoS_2	103	64	3	10	96	75	94	293	25	10	Upper plateau cell assembled uncharged. Negative electrode, pressed Al wire; positive electrode, hot-pressed. Terminated.
R-25	Li-Al/ FeS_2+CoS_2	129	83	5	8	100	78	38	65	33	50	Upper plateau cell assembled uncharged. Negative electrode, pressed Al wire, partially charged with Li foil, positive electrode, hot-pressed. Terminated.
R-26	Li-Al/ FeS_2-CoS_2	103	87	5	6	100	75	>93	>220	50	45	Upper plateau cell assembled uncharged. Negative electrode, pressed Al wire, partial charged; positive electrode, hot-pressed.
R-27	Li-Al/ FeS_2+CoS_2	85	79	5	8	99	58	>58	>192	50	50	Upper plateau cell assembled uncharged. Negative electrode, pressed Al wire, partially charged with Li foil; positive electrode, hot-pressed.
R-28	Li-Al/ FeS_2+CoS_2	200	91	3	9	91	69	>32	>76	0	0	Upper plateau cell assembled uncharged. Negative electrode, pressed Al wire, partially charged with Li foil; positive electrode, hot-pressed, contains acetylene black.
VB-1	Li-Al/ FeS_2	43	27	5	6	100	58	>13	>14	25	55	Upper plateau cell assembled uncharged. Negative electrode, pressed Al wire, partially charged with Li-Al plaque; positive electrode, hot-pressed Li_2FeS_2.

[a] Based on at least five cycles.

[b] Based on at least 10 cycles at the 5-hr rate.

[c] The "greater than" symbols denote continuing operation.

[d] Percent decline from maximum capacity at the 5-hr rate, except where noted.

APPENDIX A. (Cont'd)

Cell or Battery No.	Type of Cell	Operating Characteristics: Capacity, A-hr: Theor.	Operating Characteristics: Capacity, A-hr: Max.[a] at Indicated Rates	Operating Characteristics: Rates, hr: Disch.	Operating Characteristics: Rates, hr: Charge	Initial Eff.,[b] %: A-hr	Initial Eff.,[b] %: W-hr	Life Characteristics: Days[c]	Life Characteristics: Cycles[c]	Life Characteristics: % Decline in: Capacity[d]	Life Characteristics: % Decline in: A-hr Eff.	Remarks
VB-2	Li-Al/ FeS_2	45	24	3	6	100	71	>45	>77	50	50	Upper plateau, uncharged cell completely assembled in air. Negative electrode, pressed Al wire, partially charged with Li-Al plaque; positive electrode, hot-pressed Li_2FeS_2.
CB-1	Li-Al/ $CuFeS_2$	147	67	5	5	98	67	>427	>736	15	5	Charged, carbon-bonded $CuFeS_2$ electrode, hot-pressed Li-Al negative electrode. Open cell is sealed furnace well. Performance stable.
SS-1	Li-Al/ $FeS-Cu_2S$	650	432	11	11	100	85	>179	>195	30	3	Assembled charged; carbon-bonded $FeS-Cu_2S$ and Li-Al in Fe Retimet; designed for SES application; 3 mΩ resistance.
EM-1	Li-Al-In/ $FeS-Cu_2S$	70	46	6	6	97	82	159	318	30	11	Charged Eagle-Picher $FeS-Cu_2S$ positive electrode; Li-Al-4 wt % In negative electrode; 7.3 mΩ resistance. Terminated.
EM-3	Li-Al-Sn/ $FeS-Cu_2S$	70	57	7	7	99	85	>109	>185	10	10	Charged Eagle-Picher $FeS-Cu_2S$ positive electrode; Li-Al-8 wt % Sn negative electrode. Initial cycles showed very rapid break-in. 7.3 mΩ resistance.
M-1	Li-Al/ FeS_2-CoS_2	146	99 144 137	2 5 11	9 11 12	88 (85 (95	64 90) 78)	17	17	0	0	Sealed, charged, hot-pressed FeS_2-CoS_2 and Li-Al (55 at. % Li). Welded Mo positive terminal to current collector. Honeycomb current collectors in both electrodes. 4.3 mΩ typical resistance (as low as 2.7 mΩ), specific energy >100 W-hr/kg at 5-hr rate. Terminated.
4-2	Li-Al/ FeS_2-CoS_2	145	141 136	5 11	12 12	95 (98	68 79)	>14	>15	0	0	Sealed, charged, hot-pressed FeS_2-CoS_2 and Li-Al (55 at. % Li). Welded Mo positive terminal to current collector. Honeycomb current collectors in both electrodes. 4.3 mΩ typical resistance. Modified housing design increases specific energy to 110 W-hr/kg at 5-hr rate. Performance stable.

[a] Based on at least five cycles.

[b] Based on at least 10 cycles at the 5-hr rate.

[c] The "greater than" symbols denote continuing operation.

[d] Percent decline from maximum capacity at the 5-hr rate, except where noted.

Cell or Battery No.	Type of Cell	Operating Characteristics: Capacity, A-hr: Theor.	Max.[a] at Indicated Rates	Rates, hr: Disch.	Charge	Initial Eff.,[b] %: A-hr	W-hr	Life Characteristics: Days[c]	Cycles[c]	% Decline in: Capacity[d]	A-hr Eff.	Remarks
KK-	Li-Al/ $FeS-CuFeS_2$	120	93	5	10	99	85	>333	>460	15	0	Sealed, assembled uncharged; carbon-bonded Li_2S+Fe+Cu and Al wire plaque + Li-Al hot-pressed; 45 W-hr/kg at 2-hr rate. First sealed cell to reach 400 deep-cycle goal. Corrected feedthrough short, 99.5% A-hr efficiency, 4.5 mΩ resistance.
KK-6	Li-Al/ FeS_2-CoS_2	150	94	5	10	100	72	188	305	13	0	Sealed, assembled uncharged; carbon-bonded Li_2+Fe+CoS_2 and 32 at. % Li-Al solid plate electrodes. Testing concluded.
KK-7	Li-Al/FeS-CoS_2-TiS_2	90	79	5	10	98	78	58	85	5	8	Sealed, assembled charged; carbon-bonded positive and cold-pressed Li-Al (EP) negative. Testing of welded Mo current collector design reducing resistance to 4.5 mΩ, TiS_2 for lifetime improvement, and carbon paper particle retainer. Testing concluded.
KK-9	Li-Al/	140	110	10	10	98+	78	29	32	18	0	Sealed, assembled charged; carbon-bonded FeS_2+CoS_2 and cold-pressed Li-Al electrodes. An Eagle-Picher cell with carbon-bonded positive electrode substituted. Performance has paralleled the EP cells. Temporarily terminated.
TO-2	Li-Al/ FeS_2-CoS	119	88	16	16	75	53	11	6	50	65	Assembled uncharged; Li_2S-Fe+CoS and solid Li-Al plaque negative; Y_2O_3 felt separator/retainer, 80 mil thick, nonwelded positive current collector. Cell never stabilized, developed short. Terminated.
TO-3	Li-Al/ FeS_2-CoS		104	14	25	88	77	18	9	41.5	56	Positive and negative electrodes same as in Cell TO-2. BN felt separator/retainer approx. 110 mil thick. Nonwelded positive current collector. Developed short. Terminated.
TO	Li-Al/ FeS_2-CoS	115	-	23	23	-	-	28	-	-	-	Positive and negative electrodes same as in Cell TO-2. Zirconia cloth embedded with BN powder and BN fibers, 50 mil thick. Nonwelded positive current collector, never stabilized, temporarily terminated.

[a] Based on at least five cycles.

[b] Based on at least 10 cycles at the 5-hr rate.

[c] The "greater than" symbols denote continuing operation.

[d] Percent decline from maximum capacity at the 5-hr rate, except where noted.

APPENDIX A. (Cont'd)

Cell or Battery No.	Type of Cell	Operating Characteristics: Capacity, A-hr: Theor.	Operating Characteristics: Capacity, A-hr: Max.[a] at Indicated Rates	Operating Characteristics: Rates, hr: Disch.	Operating Characteristics: Rates, hr: Charge	Initial Eff.,[b] %: A-hr	Initial Eff.,[b] %: W-hr	Life Characteristics: Days[c]	Life Characteristics: Cycles[c]	Life Characteristics: % Decline in: Capacity[d]	Life Characteristics: % Decline in: A-hr Eff.	Remarks
TO-5	Li-Al/ FeS_2-CoS	115	104	21	21	98	83	22	25	0	15	Positive and negative electrodes same as in TO-2. BN felt separator/retainer, 110 mil thick. Welded positive current collector Developed short. Terminated.
TO-6	Li-Al/ FeS_2-CoS	105	90	4.5	16	∿99	84	>26	>29	45	45	Assembled uncharged upper plateau, Li_2S + FeS+CoS positive and Al demister wire + lithium foil negative. Welded positive current collector. BN felt separator/ retainer, 150 mil thick. Presently in operation.
						BATTERY TESTS						
B7-S	Li-Al/ FeS-Cu_2S	149	100 77 57 35	10.0 5.1 2.8 1.4	8.5 6.2 4.1 3.5	99	80	>295	>472	21	∿2	Two Eagle-Picher thick electrode cells in series. Total life of 1B4 is 344 days, 516 cycles; 1B6, 318 days, 509 cycles. Now being operated with charge plus equalization.
B9-S	Li-Al/ FeS-Cu_2S	69	53 51 49	7 5.1 3.2	7 5 4.9	98+	83	60	164	∿49	0	Two Eagle-Picher thin electrode cells (1A7, 1A8) in series. Cycled with bulk charge only. Voluntarily terminated.
B10-S	Li-Al/ FeS_2+CoS_2	156	113 97	11.3 6.5	11.3 9.7	99+	80	>23	>19	0	0	Six Eagle-Picher thick electrode cells (I-5-1, 3, 4, 5, 7, 8) is series. Started up and conditioned.

[a] Based on at least five cycles.

[b] Based on at least 10 cycles at the 5-hr rate.

[c] The "greater than" symbols denote continuing operation.

[d] Percent decline from maximum capacity at the 5-hr rate, except where noted.

APPENDIX B.

STATISTICAL DATA ON CELL AND BATTERY TESTS

Table B-1 shows the status of twenty-three experimental and industrial contractors' cells that were operated during January-March 1977. As can be seen from the table, tests of some of these cells were terminated during this period; the other cells are still in operation.

Table B-1. Status of FeS and FeS_2 Cells

Cause of Failure	FeS Cells		FeS_2 Cells		Total Cells	
	No.	%	No.	%	No.	%
Extrusion of Electrode Material	1	9	3	25	4	17
Cutting of Separator	1	9	1	8	2	9
Unknown[a]	2	18	0	0	2	9
Not Yet Examined	0	0	5	42	5	22
Operation Continuing	7	64	3	25	10	43

[a]Short circuit; cause not identified.

Table B-2 shows the highest performance and lifetime achieved by the FeS and FeS_2 cells operated during January-March 1977. The numbers in parentheses indicate the discharge rate in hours.

Table B-2. Highest Cell Performance

Cell Type and Number	Specific Energy W-hr/kg	Specific Power W/kg	Cycles
FeS, I-3-B-1	67 (10)	--	--
FeS, 1B4	60 (10)	--	516[a]
FeS, CB-1	--	--	700[a,b]
FeS_2, 2B7	65 (4)	--	400
FeS_2, 2A5	--	68	--
FeS_2, M-1	100 (5)	140	--

[a]Operation continuing at end of reporting period.

[b]Elapsed time, 402 days.

Figure B-1 depicts the number of cycles achieved by the FeS and FeS_2 cells in Table B-1. The cycle life data of Fig. B-2 were derived from the data in Fig. B-1. The mean cycle life is 294 cycles for the FeS cells and 209 cycles for the FeS_2 cells. However, these values have very large standard deviations that result from the numerous cell designs involved. A description of the cell designs and operating conditions appears in Appendix A.

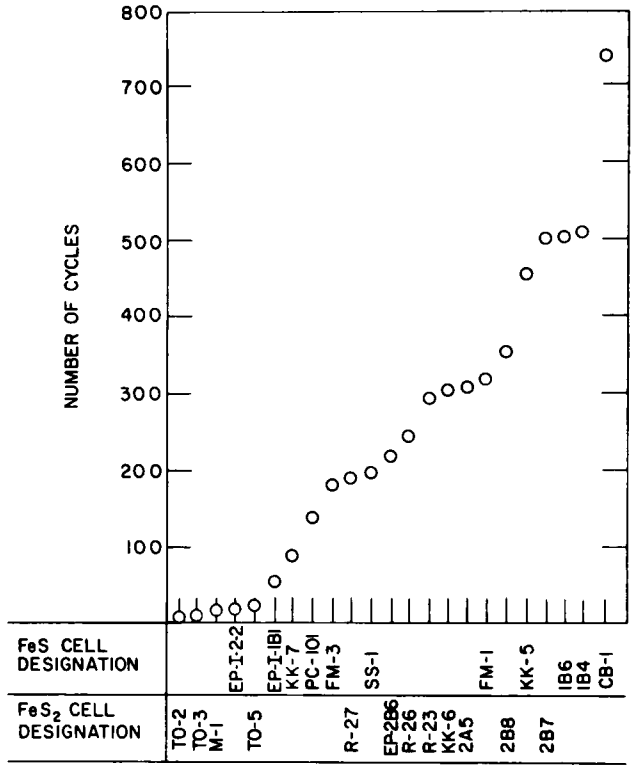

Fig. B-1. Cycle Life Data of FeS and FeS_2 Cells

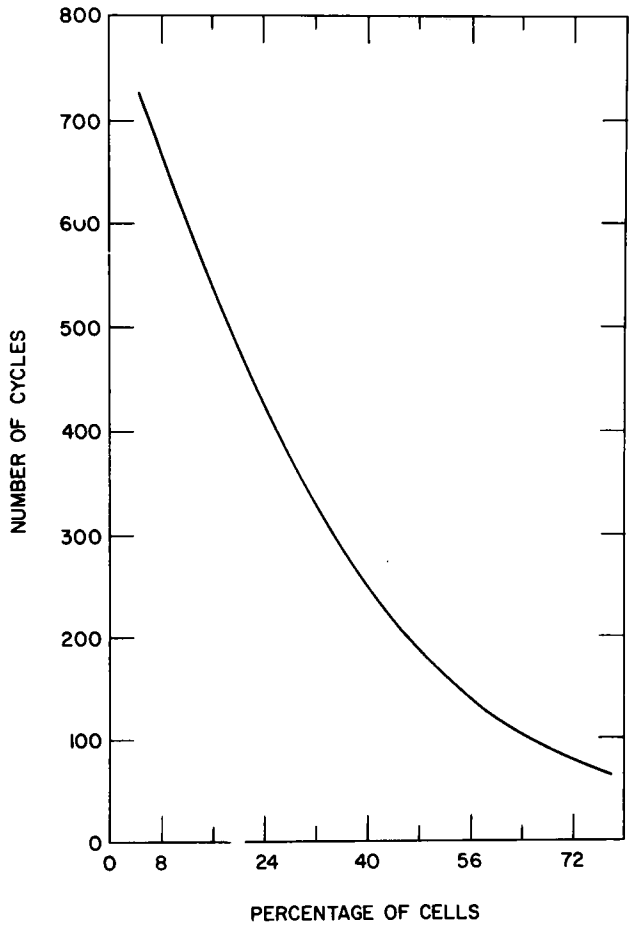

Fig. B-2. Number of Cycles *vs.* Percentage of Cells

Distribution of ANL-77-35

Internal:

M. V. Nevitt
R. V. Laney
P. R. Fields
S. A. Davis
B. R. T. Frost
G. T. Garvey
D. C. Price
K. E. Anderson
J. D. Arntzen
J. Barghusen
L. Bartholme
J. E. Battles
E. C. Berrill
W. Borger
C. A. Boquist
L. Burris
F. A. Cafasso
A. A. Chilenskas
K. Choi
P. Cunningham
D. Day
W. DeLuca
R. Dunne
J. G. Eberhart
R. Elliott
W. R. Frost
E. C. Gay
J. Harmon
F. Hornstra
A. A. Jonke
R. W. Kessie
G. M. Kesser
V. M. Kolba
W. Kremsner
M. L. Kyle
W. W. Lark
S. Lawroski
R. F. Malecha
A. E. Martin
F. J. Martino
C. A. Melendres
A. Melton
W. E. Miller
F. Mrazek
K. M. Myles
T. Olszanski
P. A. Nelson (100)
E. G. Pewitt
E. R. Proud
S. Preto
G. Redding
M. F. Roche
L. E. Ross
W. W. Schertz
J. L. Settle
H. Shimotake
J. A. Smaga
R. K. Steunenberg
B. Swaroop
C. A. Swoboda
Z. Tomczuk
R. Varma
D. R. Vissers
S. Vogler
W. J. Walsh
D. S. Webster
S. E. Wood
N. P. Yao
P. Eshman
J. E. A. Graae
J. L. Hamilton
P. A. Eident
T. D. Kaun
J. E. Kincinas
K. Kinoshita
Z. Nagy
K. A. Reed
M. A. Slawecki
N. Otto
C. Sy
A. B. Krisciunas
ANL Contract Copy
ANL Libraries (5)
TIS Files (6)

External

ERDA-TIC, for distribution per UC-94c (182)
Chief, Chicago Patent Group
V. Hummel, ERDA-CH
President, Argonne Universities Association
Chemical Engineering Division Review Committee:
- R. C. Axtmann, Princeton Univ.
- R. E. Balzhiser, Electric Power Research Institute
- J. T. Banchero, Univ. Notre Dame
- D. L. Douglas, Gould Inc.
- P. W. Gilles, Univ. Kansas
- R. I. Newman, Allied Chemical Corp.
- G. M. Rosenblatt, Pennsylvania State Univ.

J. G. Ahlen, Illinois Legislative Council, Springfield
J. Ambrus, Naval Surface Weapons Center
J. N. Anand, Dow Chemical Co., Walnut Creek, Calif.
F. Anson, California Inst. Technology
P. Auh, Brookhaven National Laboratory
B. S. Baker, Energy Research Corp.
H. Balzan, Tennessee Valley Authority
K. F. Barber, Div. Transportation Energy Conservation, USERDA

H. J. Barger, Jr., U. S. Army MERDC, Fort Belvoir
T. R. Beck, Electrochemical Technology Corp., Seattle
J. A. Belding, Div. Conservation Research & Technology, USERDA
M. Benedict, Massachusetts Institute of Technology
D. N. Bennion, Univ. California, Los Angeles
J. Birk, Electric Power Research Inst.
J. Braunstein, Oak Ridge National Laboratory
M. Breiter, GE Research & Development Center
J. O. Brittain, Northwestern U.
R. Brodd, Parma Technical Center, Union Carbide Corp.
J. J. Brogan, Div. Transportation Energy Conservation, USERDA
E. Brooman, Battelle Memorial Institute, Columbus
D. M. Bush, Sandia Laboratories
E. Buzzelli, Westinghouse Electric Corp., Pittsburgh
E. J. Cairns, General Motors Research Lab., Warren, Mich.
E. Carr, Eagle-Picher Industries, Joplin
P. Carr, Energy Development Associates, Madison Heights, Mich.
Chloride Systems (U. S. A.) Inc., North Haven, Conn.
C. Christenson, Gould Inc.
M. Cohen, Univ. of Chicago
A. R. Cook, Int'l Lead Zinc Research Organization, Inc., New York City
D. R. Craig, Hooker Chemical Corp.
G. Cramer, Southern California Edison, Rosemead
F. M. Delnick, Sandia Labs.
W. Dippold, Div. Transportation Energy Conservation, USERDA
J. Dunning, General Motors Research Lab., Warren, Mich.
P. Eggers, Battelle Memorial Institute, Columbus
M. Eisenberg, Electrochimica Corp.
R. P. Epple, Div. Physical Research, USERDA
P. L. Fleischner, National Beryllia Corp.
J. H. B. George, Arthur D. Little, Inc.
J. Giner, Tyco Labs., Inc., Waltham, Mass.
C. Goddard, Div. Conservation Research and Technology, USERDA
G. Goodman, Globe-Union, Inc., Milwaukee
G. Gorten, Gorten and Associates, Sherman Oaks, Calif.
H. Grady, Foote Mineral Co., Exton, Pa.
S. Gratch, Birmingham, Mich.
D. Gregory, Institute of Gas Technology, Chicago
N. Gupta, Ford Motor Co.
N. Hackerman, Rice U.
G. Hagey, Div. of Energy Storage Systems, USERDA
R. Hamilton, Carborundum Co., Niagara Falls
W. Hassenzahl, Los Alamos Scientific Laboratory
L. A. Heredy, Atomics International
B. Higgins, Eagle-Picher Industries, Joplin
R. Hudson, Eagle-Picher Industries, Joplin
J. R. Huff, U. S. Army Mobility Equipment R&D Center, Fort Belvoir
R. A. Huggins, Stanford U.
R. A. Huse, Public Service Electric & Gas Co., Newark, N. J.
S. D. James, U. S. Naval Surface Weapons Center (3)
M. A. Jansen, Allegheny Power Service Corp., Greensburgh, Pa.
G. Janz, Rensselaer Polytechnic Inst.
H. Jensen, C&D Batteries, Plymouth Meeting, Pa.
F. Kalhammer, Electric Power Research Institute

K. Kinsman, Ford Motor Co.
R. Kirk, Div. Conservation Research & Technology, USERDA
K. W. Klunder, Div. of Energy Storage Systems, USERDA
J. Lagowski, Detroit Edison Utility Co.
J. J. Lander, Air Force Aero Propulsion Lab., Wright-Patterson AFB
A. Landgrebe, Div. of Energy Storage Systems, USERDA (6)
C. E. Larson, Bethesda, Md.
S. H. Law, Northeast Utilities, Hartford, Conn.
H. Leribaux, Texas A&M U.
D. Linden, U. S. Army Electronics Command, Fort Monmouth, N. J.
R. Llewellyn, Indiana State U.
P. S. Lykoudis, Purdue Univ.
C. J. Major, PPG Industries, Inc.
G. Mamantov, U. Tennessee
J. McKeown, Office of Program Administration, USERDA
C. McMurty, Carborundum Co., Niagara Falls
R. McRae, ILC Technology, Sunnyvale, Calif.
D. Meighan, C. & D. Batteries, Plymouth Meeting, Pa.
R. Minck, Ford Motor Co.
F. Moore, Div. of Energy Storage Systems, USERDA
G. Murray, Detroit Edison Utility Co.
E. Nicholson, Esso Research & Engineering Corporate Res. Lab., Linden, N. J.
C. Pax, Div. Transportation Energy Conservation, USERDA
G. F. Pezdirtz, Div. of Energy Storage Systems, USERDA
R. Rightmire, Standard Oil of Ohio, Cleveland
R. Rizzo, Globe-Union Inc., Milwaukee
N. Rosenberg, Transportation Systems Center, Cambridge, Mass.
N. W. Rosenblatt, E. I. duPont de Nemours & Co., Wilmington
R. Rubischko, Gould Inc.
A. Salkind, ESB Inc., Yardley, Pa.
G. Scharbach, American Motors General Corp., Wayne, Mich.
T. Schneider, Public Service Electric & Gas Co., Newark, N. J.
R. I. Schoen, National Science Foundation
J. R. Schorr, Battelle Memorial Institute, Columbus
D. R. Schramm, Public Service Electric & Gas Co., Newark, N. J.
H. J. Schwartz, NASA Lewis Research Center
J. R. Selman, Illinois Institute of Technology
A. I. Snow, Atlantic Richfield Co., Harvey, Ill.
S. Srinivasan, Brookhaven National Laboratory
D. Stakem, Catalyst Research Corp., Baltimore
E. Steeve, Commonwealth Edison Co., Chicago
R. H. Strange II, National Science Foundation
R. L. Strombotne, U. S. Dept. Transportation, Washington
S. Sudar, Atomics International
R. H. Swoyer, Pennsylvania Power and Light Co., Allentown
F. Tepper, Catalyst Research Corp., Baltimore
L. Thaller, NASA Lewis Research Center
G. M. Thur, Div. Transportation Energy Conservation, USERDA
C. W. Tobias, U. California, Berkeley
L. Topper, National Science Foundation
W. Towle, Globe-Union, Inc.
J. Vanderryn, Office of Intern. R&D Programs, USERDA
J. V. Vinciguerra, Eagle-Picher Industries, Joplin
R. D. Walker, Jr., U. Florida

C. O. Wanvig, Jr., Globe Union, Inc., Milwaukee
S. A. Weiner, Ford Motor Co.
J. Werth, ESB Inc., Yardley, Pa.
C. Wienlein, Globe-Union Inc., Milwaukee
F. Will, General Electric R&D Center, Schenectady
J. Withrow, Chrysler Corp., Detroit
W. L. Wonell, U. of California, Berkeley
S. Wood, La Grange Park, Ill.
T. Wydeven, NASA Ames Research Center
O. Zimmerman, Portland General Electric Co., Portland, Ore.
M. Zlotnick, Div. Conservation Research and Technology, USERDA
Chloride Technical Limited, Manchester, England
E. Aiello, U. of Chicago
W. J. Argersinger, Jr., U. of Kansas
J. T. Banchero, U. of Notre Dame
K. J. Bell, Oklahoma State U.
R. Blanco, Oak Ridge Nat. Lab.
C. F. Bonilla, Columbia U.
W. Brandt, U. of Wisconsin-Milwaukee
A. E. Dukler, U. of Houston
W. J. Frea, Michigan Tech. U.
C. D. Harrington, Douglas United Nuclear, Inc.
J. E. Linehan, Marquette U.
Maine Univ., Prof. in charge of Chem. Engr. Lib.
Marquette U., Dept. of Chemistry
Michigan Tech. U., Library
G. Murphy, Iowa State U.
E. A. Peretti, U. of Notre Dame
G. W. Preckshot, Engr. U. of Missouri
H. Rosson, U. of Kansas
C. Sanathanan, U. of Illinois-Chicago Circle
A. Sesonske, Purdue U.
USERDA, Director, Div. of Safeguards and Security
B. W. Wilkinson, Michigan State U.
Comision Nacional de Energia Atomica, Library, Argentina
J. A. Sabato, Com. Nac. de Energia Atomica, Buenos Aires, Argentina
C. H. Cheng, Nat'l Tsing Hua Univ., China
National Radiological Protection Board, Library, Harwell, England
L. Kemmerich, Ges. fur Kernforschung, Karlsruhe, Germany
F. Weigel, Inst. fur Anorganische Chemie der U. Munich, Germany
N. Saratchandran, Bhabha Atomic Research Centre, Bombay, India
K. Fujimiya, U. of Tokyo, Japan
Japan Atomic Energy Research Inst., Tokai-mura, Japan
K. Matsuda, Inst. of Physical & Chemical Res., Yamato-machi, Japan
Sang-Soo Lee, Korea Advanced Institute of Science, Korea
Korean Atomic Energy Research Institute, Korea
Ragnar Nordberg, Sahlgren's Hospital, Goteborg, Sweden